Chapter 6
Structural and Functional Properties of Viral Membrane Proteins

Bo OuYang, Ying Dong, and James J. Chou

Abstract Viruses have developed a large variety of transmembrane proteins to carry out their infectious cycles. Some of these proteins are simply anchored to membrane via transmembrane helices. Others, however, adopt more interesting structures to perform tasks such as mediating membrane fusion and forming ion-permeating channels. Due to the dynamic or plastic nature shown by many of the viral membrane proteins, structural and mechanistic understanding of these proteins has lagged behind their counterparts in prokaryotes and eukaryotes. This chapter provides an overview of the use of NMR spectroscopy to unveil the transmembrane and membrane-proximal regions of viral membrane proteins, as well as their interactions with potential therapeutics.

6.1 Introduction

We will focus our discussion on two classes of transmembrane (TM) proteins encoded by viruses, viroporins (or viral channels) and membrane fusion proteins, as these proteins have been sought after as antiviral targets and they often exhibit peculiar structural features not seen in other membrane proteins. As implied by their name, the viroporin proteins can form channel-like structures in lipid bilayer that permeate ions or solutes. Now over a dozen viroporins from various sources have

B. OuYang (✉) · Y. Dong
State Key Laboratory of Molecular Biology, National Center for Protein Science Shanghai, CAS Center for Excellence in Molecular Cell Science, Shanghai Science Research Center, Shanghai Institute of Biochemistry and Cell Biology, Chinese Academy of Sciences, Shanghai, China

University of Chinese Academy of Sciences, Shanghai, China
e-mail: ouyang@sibcb.ac.cn

J. J. Chou (✉)
Department of Biological Chemistry and Molecular Pharmacology, Harvard Medical School, Boston, MA 02115, USA
e-mail: james_chou@hms.harvard.edu

Y. Cao (ed.), *Advances in Membrane Proteins*,
https://doi.org/10.1007/978-981-13-0532-0_6

been characterized, covering a wide range of ion substrates including H^+, K^+, Na^+, Ca^{2+}, and Cl^-, as well as larger substrates such as RNA. The exact function of ion channel activity in many viruses is not yet known, though their roles have been implicated in entry, virus assembly and virus release. The function of membrane fusion proteins is much better defined, that is, to enable viral entry by mediating virus-host membrane fusion. The viral fusion proteins have large extramembrane domains for receptor recognition and for grabbing onto the host cell membrane, but the function of their TM and membrane-proximal regions have been elusive. Functional mutagenesis studies have suggested that, at least in the cases of HIV-1 and influenza A viruses, the TM domains (TMDs) of fusion proteins are not merely membrane anchors, but play important roles in membrane fusion and viral infectivity. Apart from the channels and fusion proteins, some viruses have developed enzymatic domains anchored to the membrane, e.g., the polymerases of the hepatitis C virus and the neurominidase of the influenza viruses. In these cases, the TMDs are believed to only serve as membrane anchors and thus will not be discussed in this chapter.

6.1.1 Function of Viroporins

Viroporins serve highly diverse functions in viral infection cycles (illustrated in Fig. 6.1). Early studies of viroporins have focused on only a few systems including 2B of poliovirus, 6K of togavirus, and M2 from influenza A virus (AM2). The 2B is a well-known viroporin that can modify membrane permeability and allow the passage of ions and small molecules during later stages of viral infection [1–3]. The 6K is a small, hydrophobic acylated protein that has been shown to form cation-selective channels when inserted into lipid bilayers [4]. The 6K is proposed to be involved in virus budding, but the exact role of 6K in the viral life cycle is poorly characterized [5–7]. The AM2 proton channel is the most studied viroporins because (1) it is the drug target of the first anti-flu drug (amantadine or rimantadine) and (2) it is one of the smallest proton channels with proton selectivity motif not found in any of the proton channels from other organisms [8–10]. Since the definition of viroporin has been put forward, more and more viroporins have been classified (Table 6.1). The influenza B virus encodes the BM2 proton channel that is a functional homolog of the AM2 but cannot be blocked by the adamantane family of drugs [11]. The human immunodeficiency virus type 1 (HIV-1) Vpu and the hepatitis C virus (HCV) p7 have been shown to form oligomeric channels to conduct cations [12–16]. The 2B protein from the enterovirus 71 (EV71), however, displayed altered channel activity, as it conducts anions (e.g., Cl^-) instead of cations [17]. Paramecium bursaria chlorella virus 1 (PBCV-1) has a viral K^+ channel named Kcv that contains the canonical potassium selectivity filter [18] and was proposed to adopt similar structure as KcsA [19]. In addition to the ion channels, the VP4 from rhinovirus can form pores that

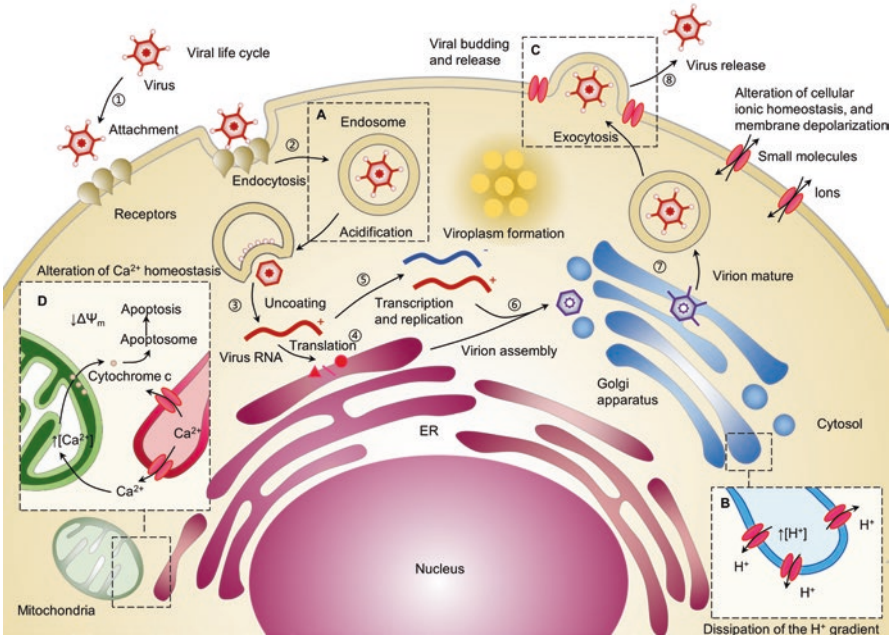

Fig. 6.1 Life cycle of virus and functions of viroporins. (*1*). Virion attaches directly host cell receptors on the membrane (*2*). and subsequently enters the cell by receptor-mediated endocytosis (*3*). Acidification of the endosomal vesicles triggers conformational changes in the virion, resulting in fusion between the viral and the endosomal membranes, allowing the release of the nucleocapsid into the cytoplasm. The viral RNA is then released into the cytoplasm and presented to the endoplasmic reticulum (ER) (*4*). At the ER, viral RNA is translated into protein that is processed by viral and host proteases (*5*). After the viral replication complex is synthesized, RNA synthesis begins by the transcription of an antisense viral RNA followed by the amplification of viral RNA (*6*). The newly synthesized RNA is subsequently packaged by capsid protein, forming a nucleocapsid (*7*). Virus assembly occurs on the surface of the ER when the nucleocapsid buds into the ER lumen, then transported through the Golgi, where acidification induces virus maturation (*8*). Mature viral particles are released in the neutral pH of the extracellular millieu

(*A*) viral entry, which acidifies the virion interior immediately after endocytosis and facilitates RNA release

(*B*) Dissipation of the proton gradient in the Golgi and the *trans*-Golgi network. The viroporins influenza A virus (IAV) matrix protein 2 (M2) and hepatitis C virus (HCV) p7 equilibrate the proton concentration with the cytosol to reduce the acidification of vesicular acidic compartments

(*C*) viroporins play an essential role in assembly, budding and release of the viral particles

(*D*) Alteration of cellular Ca^{2+} homeostasis. Calcium uptake by the mitochondria can lead to dissipation of the inner-mitochondrial-membrane potential ($\Delta\Psi m$), permeabilization of the outer mitochondrial membrane and, finally, the release of cytochrome *c*. In the cytosol, cytochrome *c* promotes the subsequent formation of apoptosome that is involved in apoptosis

Table 6.1 List of identified viroporin proteins[a]

Name of virus	Names of viroporin	# of amino acid	Oligomeric state	Conducting ion	References
Influenza A virus	AM2	97	Tetramer	Proton	[74, 153]
Influenza B virus	BM2	115	Tetramer	Proton	[75, 154]
Hepatitis C virus	p7	63	Hexamer/ heptamer	Cation	[15, 99, 155]
HIV-1	Vpu	81	Pentamer	Cation	[156, 157]
SARS-CoV	3a	274	Tetramer	K^+	[158]
	E	76	Pentamer	Na^+ over K^+	[159]
Poliovirus	Vp4	68	N/A[b]	RNA	[20, 160]
	2B	97	Dimer/tetramer	Ca^{2+}	[3, 161]
Togavirus	6 k	60	N/A[b]	Cation	[4]
Enterovirus	2B	99	Dimer/tetramer	Cl^-	[17]
HPV	E5	83	N/A[b]	N/A[b]	[162–164]
PBCV-1	Kcv	94	Tetramer	K^+	[18, 165]

[a]The viruses listed are influenza A virus (IAV), influenza B virus (IBV), hepatitis C virus (HCV), human immunodeficiency virus type 1 (HIV-1), severe acute respiratory syndromes-associated coronavirus (SARS-CoV), alphavirus, poliovirus, human papilloma virus (HPV), and Paramecium bursaria chlorella virus 1 (PBCV-1)

[b]Pore formation indicated but a defined oligomeric state either does not exist or is not characterized

allow single-stranded viral RNA to cross the membrane [20, 21], further expanding the list of substrates that viroporins transport.

Probably the best-defined roles of viroporins are that of the M2 proton channels of influenza A and B viruses, both of which involve equilibrating pH between compartments. One important role of the M2 is to equilibrate pH across the viral membrane during viral entry, which acidifies the virion interior immediately after endocytosis and facilitates RNA release [22, 23] (Fig. 6.1a). Another role of M2 is to equilibrate pH across the trans-Golgi membrane of the infected cells during viral maturation, which preserves the pre-fusion form of the hemagglutinin fusion protein through de-acidification of the Golgi lumen [24] (Fig. 6.1b). The roles of other cation-selective viroporins are less clear. One of the general roles proposed for viroporin is to depolarize either the ER or plasma membrane to facilitate membrane curvature formation during virus budding [25, 26] (Fig. 6.1c). In the case of HCV, for example, the p7-mediated channel activity has been reported to facilitate virus release [27, 28]. Another general role for viroporin is simply to cause cation leakage, which would induce cellular stress and programmed cell death [29] (Fig. 6.1d). In addition to ion permeation, several viroporins are known to participate in viral assembly through interaction with other proteins. For example, the influenza AM2 and BM2 proteins both have significant cytoplasmic domains that are believed to recruit matrix proteins M1 during virus assembly [30–32]. The HCV p7 protein has also been reported to interact with other non-structural proteins such as NS2, and this interaction appears to be crucial for the production of infectious HCV particles [33, 34].

6.1.2 Viral Membrane Fusion Proteins

Enveloped viruses infect host cells by the fusion of viral and cellular membrane. Depending on the type of the virus, fusion can occur either with the host plasma membrane or with the endosomal membrane. The membrane fusion must occur without consuming energy; it is catalyzed by major conformational changes of specialized envelope proteins generally known as viral fusion proteins. Despite their diversity, all known viral fusion proteins convert from a prefusion state (dimers or trimers, depending on the class), through a key intermediate state (extended conformation), to a postfusion state (a trimer of hairpins) that brings the fusion peptide, attached to the target membrane, and the TM domain, attached to the viral membrane, into close proximity thereby facilitating the fusion of viral and target membranes (Fig. 6.2a) [35]. Three distinct classes of viral fusion proteins (exemplified in Fig. 6.2b) have been defined based on structural criteria [36]. The Class I includes fusion proteins from some of the best characterized human pathogens, such as influenza and HIV-1. These proteins are trimers of a single chain precursor that requires a proteolytic cleavage to generate two fragments. For example, the influenza A hemagglutinin (HA) contains the N-terminal fragment HA1 and C-terminal fragment HA2 [37], and the HIV-1 envelope protein is cleaved into the gp120 and gp41 fragments [38]. The fusogenic fragment gp41 bears a hydrophobic fusion peptide capped by the outer receptor binding fragment gp120 [39]. Receptor binding accompanies cap protein release, allowing major conformational changes in the gp41 that ultimately leads to fusion [40]. In the case of influenza, the cap HA1 is released by low pH of the endosome after endocytosis [41]. The Class II fusion proteins are found on flaviviruses, alphaviruses, and bunyaviruses (E in flaviviruses, E1 in alphaviruses, GN and GC in bunyaviruses) [42, 43]. Although these fusion proteins are architecturally different from the Class I fusion proteins, i.e., Class II fusion proteins are mostly made of β-sheets as opposed to the helical structures of the Class I fusion proteins, they operate on the same physical principle. Their fusion peptides are formed as loops at the tips of β-strands that serve as an anchor to insert into the host membrane after endocytosis. Unlike Class I proteins, which remain trimeric, their conformational change involves a change in oligomeric state from pre-fusion dimers to post-fusion trimers [44, 45]. The reduced pH of the endosome induces a cascade of subsequent refolding and trimerization events that achieve membrane fusion [46]. Members of the Class III include G protein of VSV, gB of herpes simplex virus and Epstein-Barr virus (EBV), and gp64 of the insect-cell baculovirus [47]. The Class III fusion proteins combine some of the features of Class I and II fusion proteins [48]. Each protomer is composed of five domains that contain a central trimeric coiled-coil, a hallmark of Class I proteins in their post-fusion states, three of the domains are predominantly made of β-sheets and their fusion peptide more closely resemble those of Class II proteins in that their fusion loops are found at the tips of extended β-strands [49].

Due to the essential roles of viral fusion proteins during infection, they have long been pursued as targets for antiviral intervention. For example, the approved small

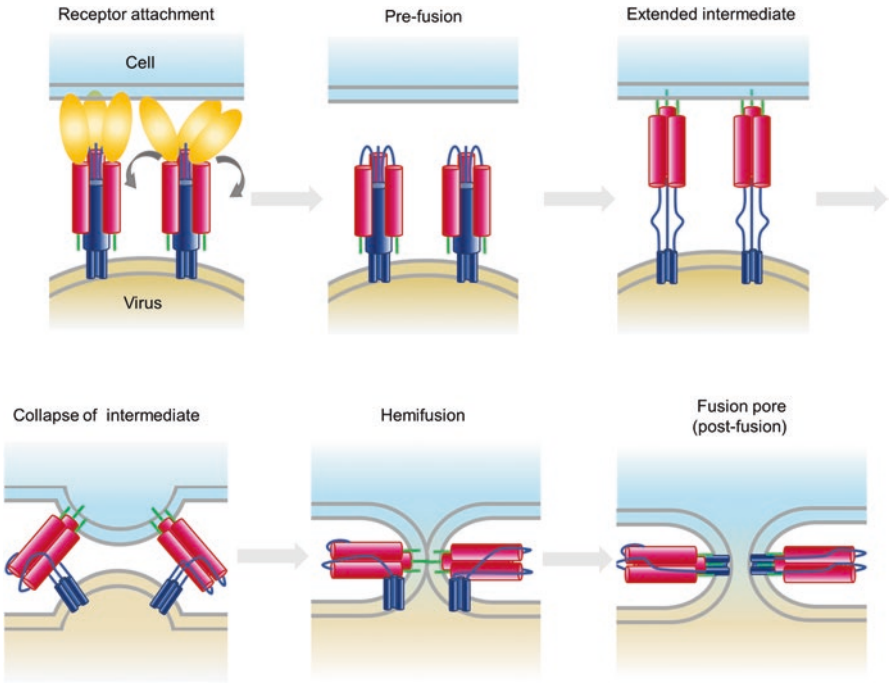

Fig. 6.2a Schematic diagram of stages of influenza virus fusion
1. Receptor attachment
2. Pre-fusion conformation, with its fusion peptide or loop (light green) sequestered
3. Extended intermediate. The fusion peptide or loop interacts with the target bilayer
4. Collapse of the extended intermediate: a C-terminal segment of the protein folds back along the outside of the trimer core. The entire trimer can bow outward, away from the deforming membrane
5. Hemifusion. The two bilayers are brought close enough into contact, the apposed, proximal leaflets merge into a hemifusionstalk
6. Fusion pore formation. Post-fusion conformation open a fusion pore

molecule drug Arbidol is used as a broad-spectrum inhibitor of influenza A and B virus, as well as hepatitis C virus [50, 51]. Unlike many other broad-spectrum antivirals, Arbidol has an established mechanism of action against the HAs in influenza A and B viruses that involves the inhibition of virus-mediated membrane fusion and thus viral entry [50]. In addition, Enfuvirtide (T20, Fuzeon) is an approved peptide drug that blocks the HIV-1 entry [52]; it is derived from the C-terminal heptad repeat 2 region of the HIV-1 gp41 envelope glycoprotein, designated the C-peptide, that disrupts membrane fusion by competing with an intra-molecular interaction that is important for the refolding of gp41 during membrane fusion [53]. Apart from being therapeutic targets, another important medical use of the fusion proteins is vaccine development. Viral fusion proteins are usually presented on the virion surface with high copy numbers, and thus are popular antigens for eliciting broad-spectrum neutralizing antibodies. For example, the native conformations of the

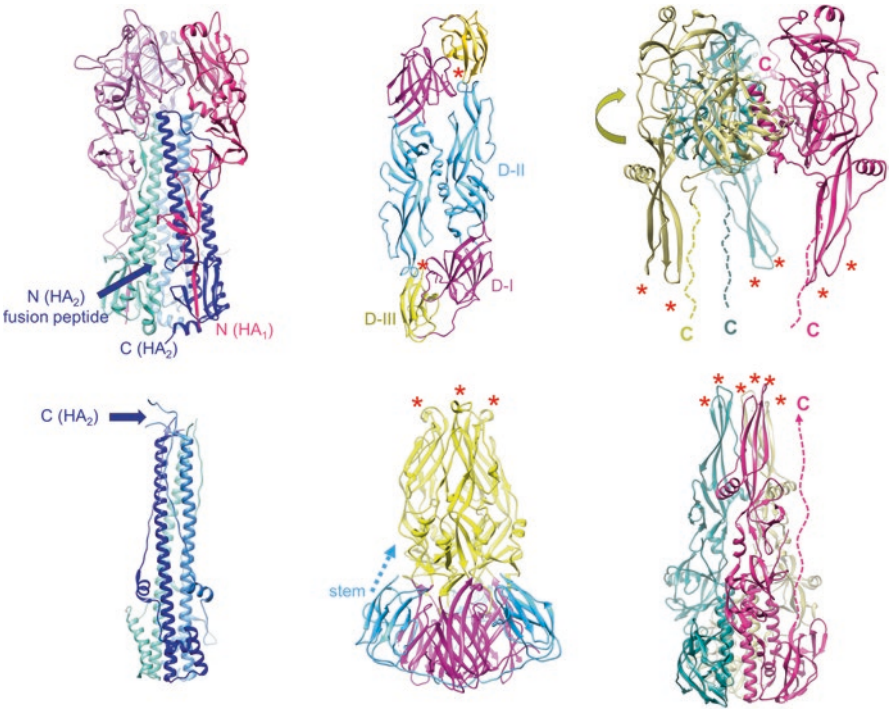

Fig. 6.2b Pre- and postfusion structures (top and bottom, respectively) of representative fusionproteins from the three known classes

Class I: influenza virus HA ectodomain (Protein Databank entries 2YPG and 1QU1 for pre- and postfusion forms of the ectodomain, respectively). HA1 chains in shades of pink/magenta and HA2 chains in shades of blue (paired as pink-cyan, dark magenta-blue, and purple-marine blue). The N terminus of HA1 and the C-terminus of the HA2 ectodomain are labeled. Blue arrow: position of fusion peptides inserted near threefold axis in prefusion form. Only HA2 is shown on the bottom. The N-terminus (blue arrow; note that the fusion peptide is not part of the structure shown) and C-terminus of the blue-colored subunit are indicated

Class II: dengue virus type 2 E protein (1OAN and 1OK8). the radial ("top") view shows just the "stem-less" ectodomain (1OAN). Colors: domain I: magenta; domain II: cyan; domain III: yellow; stem: cyan; Colors for domains I, II and III are the same in the postfusion representation. A dashed cyan arrow on the postfusion trimer shows where the stem emerges from domain III. Red asterisks: fusion loops

Class III: VSV G ectodomain (2J6J and 2CMZ). The three chains are in gold, sea green, and magenta. Dashed lines show the location of a disordered, C-terminal segment that connects the folded protein to the transmembrane anchor. Only the magenta-subunit C-terminal segment is shown on the bottom. The curved gold arrow indicates that in the transition from the conformation on the top to the conformation on the bottom, the domain bearing the fusion loops flips over by about 180° to engage the host-cell membrane. Red asterisks: fusion loops

HIV-1 envelope glycoprotein have being pursued intensely as immunogens for B-cell based vaccine development [54, 55].

6.2 Structural Methods for Investigating Viral Membrane Protein

For most single-pass TM proteins, the role of their TMDs beyond membrane anchoring is unresolved, partly because of the difficulty in structural studies: they are notorious for resisting crystallization and due to their small sizes, unfeasible for visualization by cryo-electron microscopy (EM). There have been only a few examples of crystal structures of the small TMDs, including the TMD of the AM2 [56, 57] and the more recent crystal structure of the TM helix dimer of the glycophorin A protein [58]. As cryo-EM is rapidly approaching atomic resolution, it is becoming increasingly used to examine the structures of the much larger viral fusion proteins containing the TMD. Most notably, a recent cryo-EM study of the HIV-1 envelope glycoprotein (Env) including the TMD achieved a high resolution structure of the prefusion state of the HIV-1 Env [59]. This study, however, showed that the TMD and the membrane-proximal regions of the Env are disordered, possibly due to incompatibility between the membrane-associated regions of the Env and the detergent used to solubilize the Env.

In this chapter we mainly focus on the use of NMR to study the TM and membrane-proximal regions of viral membrane proteins, including methods for structure determination and for investigating drug binding. The first challenge of NMR studies is preparing sufficient quantities of isotope labeled proteins and this is not trivial for small and hydrophobic proteins. A robust approach is to force high-level expression of the hydrophobic peptides, which are toxic to cells, into inclusion bodies. In our experience, the most effective implementation of this approach is to express the peptide as a C-terminal fusion to the trpLE protein (which drives inclusion body formation) in the pMM-LR6 vector [60–62] (Fig. 6.3a). The trpLE has an N-terminal 9×His tag to permit nickel affinity purification. A methionine between the trpLE and the peptide is added for cleavage by cyanogen bromide so that the peptide can be released from the trpLE. Purification of the peptide involves (1) purifying the trpLE-peptide fusion protein from the inclusion bodies by nickel affinity, (2) cleavage by cyanogen bromide of the fusion protein in formic acid, and (3) separation of the peptide from trpLE or fusion protein by reverse-phase HPLC. While the above protocol is quite general for hydrophobic peptides, it requires that the peptides have no methionine in the middle of the peptide sequence. If the native methionines cannot be mutated, an alternative method is to use soluble fusion domains (e.g., the maltose binding protein) with specific protease cleavage site for releasing the peptide.

The purified hydrophobic peptides can be reconstituted in any membrane mimetic media, including detergent micelles, bicelles, and lipid nanodiscs. While

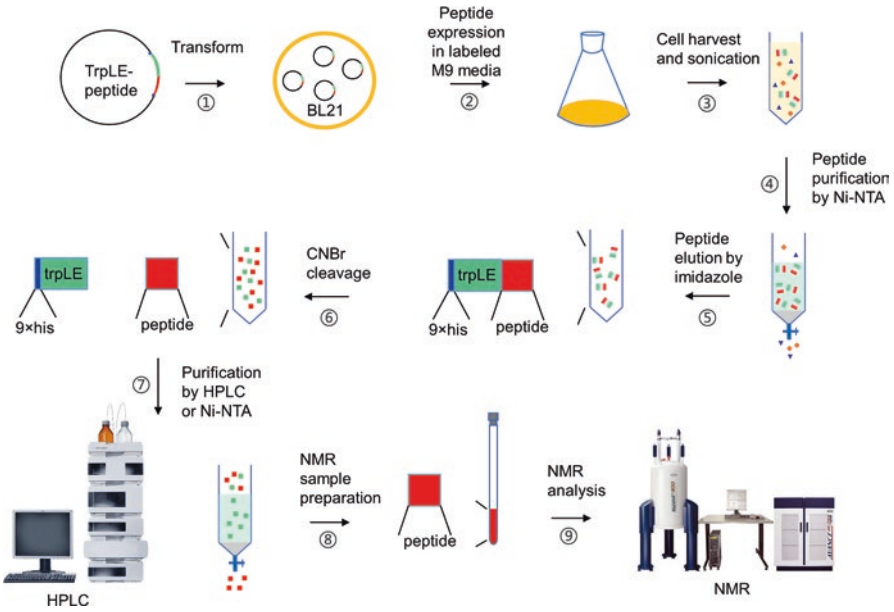

Fig. 6.3a Schematic of hydrophobic peptide sample preparation using HCV p7 as an example
1. trpLE plasmid with targeted peptide is transformed into and BL21(DE3) competent cells for expression
2. The cells were grown in M9 media
3. Cells were collected by centrifugation and lysed by sonication
4. After lysis, the inclusion bodies and membranes were collected by centrifugation and dissolved in 6 M guanadine buffer. Insoluble aggregates were removed by centrifugation. The supernatant was then subjected to Ni-NTA purification.
5. The protein was eluted using 400 mM imidazole
6. Cyanogen bromide cleavage followed by dialysis in water
7. The protein was further separated by reverse-phase HPLC or Ni-NTA
8. The lyophilized peptide was then dissolved in detergent and refolded by dialysis against the NMR buffer
9. NMR experiments were performed at spectrometers

nanodiscs are the closest mimic of native membrane, we find that the lipid/detergent bicelle system is a good compromise between having the capacity to provide a near lipid bilayer environment and generating good NMR spectra. Previous studies on the bicelle system with 1,2-dimyristoyl-*sn*-glycero-3-phosphocholine (DMPC) as lipid and (1,2-dihexanoyl-*sn*-glycero-3-phosphocholine (DHPC) as detergent have shown that when the molar ratio of lipid to detergent (q) > 0.5, the assembly reaches the ideal bicelle condition in which the lipid and detergents are well segregated [63, 64]. At $q = 0.5$, for example, the estimated diameter of the lipid bilayer region of the bicelle disc is ~45 Å according to the equation describing bicelle assembly [64–66], and this size is sufficiently large to accommodate small TMDs. Remarkably, even bicelles of such size could generate NMR spectra of sufficiently high quality to enable full-scale structure determination, as was demonstrated for the structure

determination of the trimeric TMDs of the Fas death receptor [67] and HIV-1 Env [68]. Here we provide an example of bicelle reconstitution from a previous study on the TMD of HIV-1 Env [68]. The hydrophobic peptides (lyophilized) are first completely dissolved in strong organic solvent (e.g., hexafluoro-isopropanal) with calculated amount of DMPC. The solution is slowly dried to a thin film under nitrogen stream. The dried film is then dissolved in 8 M Urea containing calculated amount of DHPC. The denaturant is removed by dialysis, during which the DMPC: DHPC ratio is monitored by 1D NMR, and the loss of DHPC during dialysis is compensated by further addition of DHPC.

Owing to the small size of most of the TMDs of viral membrane proteins, structure determination by NMR is normally straightforward. Probably the biggest challenge is measuring inter-protomer restraints in cases of oligomer complexes. In particular, structure determination of symmetric oligomers faces the challenge of measuring NOE-based ^{1}H-^{1}H distances between structurally equivalent protomers having the same NMR peaks, which are needed as inter-protomer restraints. A proven way to solve this problem is using a mixed sample in which half of the protomers are (^{15}N, ^{2}H)-labeled and the other half ^{13}C-labelled, for measuring, exclusively, NOEs between the ^{15}N-attached ^{1}H of one protomer and ^{13}C-attached ^{1}H of the neighboring protomer [60, 69] (example from the TMD of the Fas receptor shown in Fig. 6.3b). Once the trimer solution is established, conventional ^{15}N- and ^{13}C- edited NOE experiments can then be used to collect self-consistent backbone-sidechain and sidechain-sidechain NOE restraints. In addition to structure determination, an important aspect of small TMDs is interaction with membrane. The bicelle system allows accurate determination of the position of TMD in the bilayer region of the bicelles using a solvent paramagnetic relaxation enhancement (PRE) analysis [63]. In this method, titration of the water-soluble and membrane-inaccessible paramagnetic agent, Gd-DOTA (Gadolinium (III) 1,4,7,10-Tetraazacyclododecane-1,4,7,10-tetraacetate), is used to generate the solvent PRE. This approach is based on the notion that if the bicelle is sufficiently wide, the lateral solvent PRE becomes negligible, thus allowing the use of measurable solvent PRE to probe residue-specific depth immersion of the protein along the bicelle normal. At each titration point, a 2D ^{1}H-^{15}N correlation spectrum is recorded to measure residue-specific PRE. For each of the residues, the PRE titration curve is fitted to exponential decay to derive the residue-specific PRE amplitude (PRE_{amp}). The PRE_{amp} vs. (residue position) along the trimer symmetry axis (parallel to the bilayer normal) is then analyzed using *the sigmoidal fitting* method [63] to determine the TMD region that resides at the center of the bilayer as well as the thickness of the bilayer around the protein.

For studying small molecule drug binding to viral membrane proteins, chemical shift perturbation (CSP) induced by drug titration is a convenient probe for identifying the approximate binding site. But, cautions need to be taken due to complications associated with membrane-mimetic media. First, many small molecule

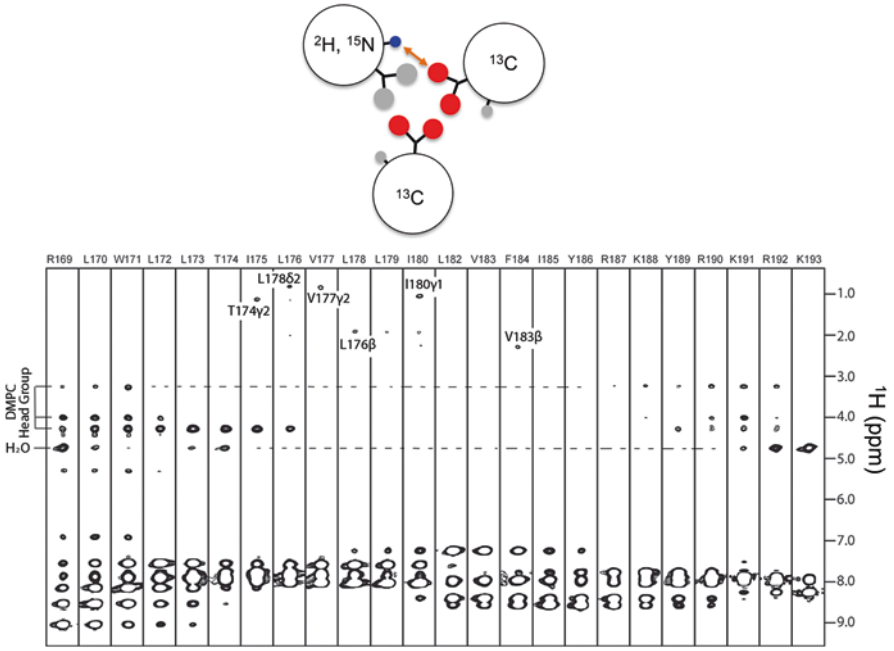

Fig. 6.3b Measurement of inter-protomer NOEs for the TMD of the mouse Fas receptor
Top: Illustration of different isotope labeled chains
Bottom: Residue-specific strips taken from the 3D ^{15}N-separated NOESY-TROSY-HSQC spectrum (NOE mixing time = 300 ms) recorded at 800 MHz using the mouse Fas-TM sample containing 50% (^{15}N, ^{2}H)-labeled peptide and 50% (15% ^{13}C)-labeled peptide. The crosspeaks in the aliphatic regions are intermonomer NOEs between the backbone amide and the sidechain methyl protons

inhibitors are hydrophobic and preferentially partition into detergent micelles or lipid/detergent bicelles, and thus the CSP can be induced simply by alteration of the micelle/bicelle environment. Second, in addition to CSP caused by close ligand contact, CSP could arise from changes in conformation and/or dynamics. Hence, the more direct NOE data is preferred wherever feasible. The simplest and the most sensitive approach for collecting protein-drug NOE is using proteins that are ^{15}N-labeled and completely deuterated so that NOE between the protein backbone amide protons and drug protons could be measured unambiguously (Fig. 6.3c). Once the binding site has been unambiguously spotted, further contacts between the drug and protein sidechains can be measured using conventional ^{13}C-edited methyl or aromatic NOESY. Details of these experiments have been described in studies that identified the drug binding sites in the influenza AM2 and HCV p7 channels [60, 70, 71].

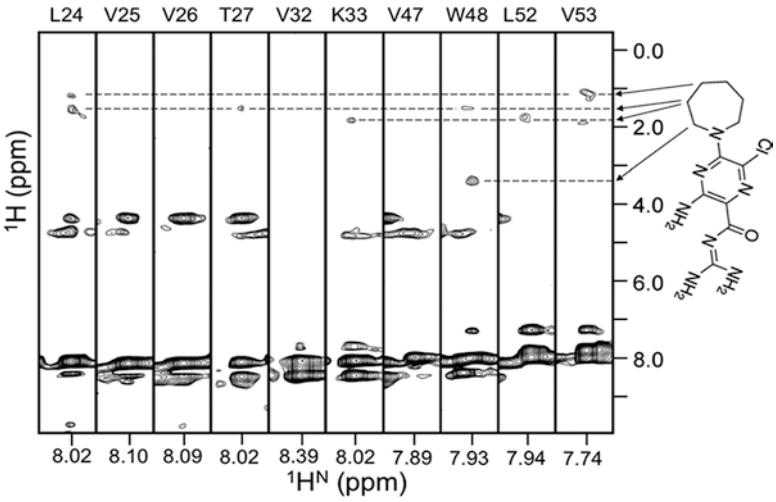

Fig. 6.3c NOESY experiments identifying the HMA binding site of p7 channel in HCV. Representative strips from the three-dimensional ^{15}N-edited NOESY TROSY spectrum (300 ms NOE mixing time) showed HMA NOEs to the backbone amide protons of Leu24, Thr27, Lys33, Trp48, Leu52, and Val53 of p7

6.3 Viroporin Architectures and Mechanism

Structural studies of viroporins have been challenging because these small membrane proteins are typically dynamic and very hydrophobic. In the past 10 years, multiple biophysical techniques including solution NMR, solid-state NMR, X-ray crystallography, and EM have been used to gradually fill the structural gaps. Taking the influenza AM2 for example, there is now structural information in crystal and solution states, in lipid bilayer, under different pHs, and bound to different small molecules. These complementary structural data allow elucidation of the functional mechanism from different view angles.

6.3.1 The Influenza M2 Channels: Structural Solutions for Proton Conduction

The AM2 of influenza A and the BM2 of influenza B are 97- and 109-residues single-pass membrane proteins, respectively, that form homotetramers in membrane [72–76]. The sequences consist of three domains: an extracellular N-terminal domain, a transmembrane domain (TMD) and an intracellular C-terminal domain. These domains arrange into different structures. The only homologous sequence

between the two proteins is the HxxxW sequence motif of the TMDs that is essential for channel activity. The TM region of the AM2 contains residues 24–46. The unstructured extracellular segment of AM2 is relatively conserved and has been sought after as a vaccine epitope [77–81]. BM2 has a similar sized TMD (residues 4–33), but a much larger C-terminal cytoplasmic domain [32, 82]. The BM2 cytoplasmic region also assembles into oligomers which are important for recruiting the matrix proteins to the cell surface during the viral assembly [30, 31, 83, 84].

The first high-resolution structures of the AM2 channel were reported concurrently by solution NMR spectroscopy and X-ray crystallography in 2008 [56, 62]. Subsequent X-ray and solution NMR studies also determined structures under different conditions [57] and with different drug resistance mutations [85, 86]. Moreover, structural characterization by solid-state NMR studies generated the channel structures in the lipid bilayer environment [87–89]. The above AM2 structures solved under different conditions show significantly different conformations (Fig. 6.4a), suggesting that the tetrameric assembly of the AM2 is quite dynamic and is sensitive to the reconstitution environment. The structural plasticity observed in AM2 is likely present in many other viral membrane proteins, which could explain why structural study of this type of proteins has been so difficult. Despite the differences, the experimental structures converged to a common mode of channel assembly: a left-handed four-helix bundle forms the channel pore, and that tetramerization of the four TM helices is further stabilized by intermolecular contacts between C-terminal amphipathic helices flanking the TMD [62, 88]. This mode of assembly places the “H” and “W” of the HxxxW sequence motif inside the channel (Fig. 6.4a). Four imidazole rings of His37, which are pH-gating features and are essential in transporting protons, are packed closely inside the pore (Fig. 6.4b). Moreover, packing of the Trp41 indoles creates a channel gate, which occludes the C-terminal end of the pore.

The structure of the BM2 channel was solved using solution NMR methods [32]. Although the overall assembly of the BM2 TMD is similar to that of the AM2 TMD, i.e., both show left-handed helical packing, the two differ substantially in details (Fig. 6.4c). Unlike the AM2, the BM2 channel shows strong coiled-coil characteristics with regular heptad repeats [8]. In the BM2 structure, the two heptad repeats show that positions *a* and *d* are occupied mostly by hydrophilic residues such as serines and His19; positions *g* and *e* are occupied by hydrophobic leucines and phenylalanines, respectively, to allow for peripheral hydrophobic interactions between the leucines and phenylalanines (Fig. 6.4d). This arrangement for coiled-coil assembly in membrane allows the TM segment to form a stable tetramer by itself and is the opposite to that of water-soluble coiled-coil tetramer, in which positions *a* and *d* are typically hydrophobic residues and positions *g* and *e* are polar residues [90]. The histidine (His19) and tryptophan (Trp23) of the HxxxW motif are also pore-lining in the inverse coiled-coil assembly in membrane. The cytoplasmic domain of the BM2 also oligomerizes into a left-handed coiled-coil tetramer, but it is water-soluble

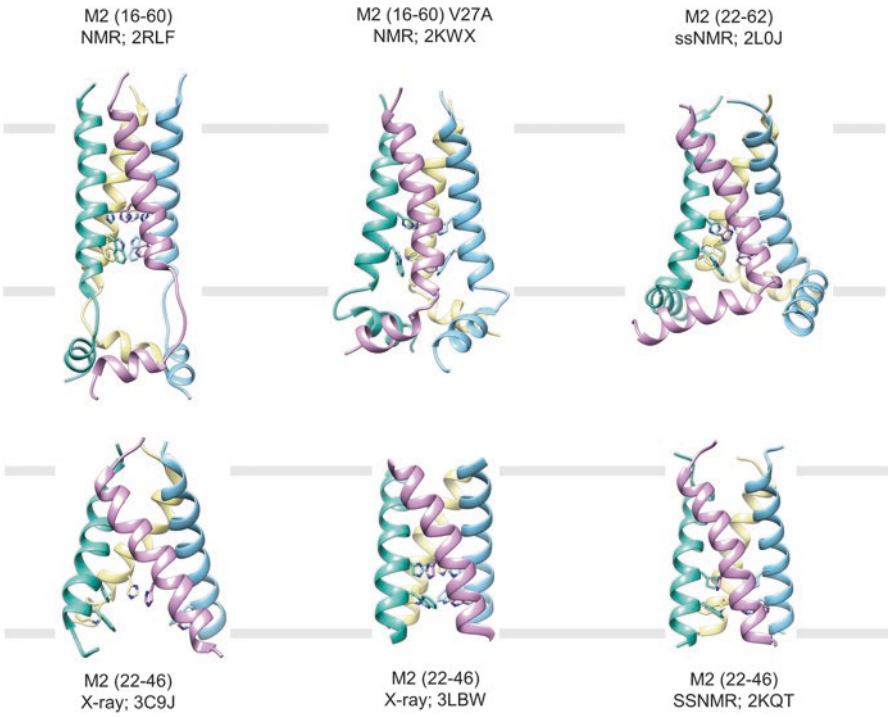

Fig. 6.4a Structures of the influenza proton channels and mechanism of proton conduction. The many structures of the influenza M2 channel. The PDB codes 2RLF and 2KWX represent the solution NMR structures of the wildtype and the V27A mutant determined using residues 18–60. The 3C9J and 3LBW are crystal structures of the TM domain (residues 22–46) determined at pH 7.3 and pH 6.5, respectively. The structures 2L0J and 2KQT were obtained using solid-state NMR using protein constructs that encompass residues 22–62 and residues 22–46, respectively

and shows strong bipolar distribution in the surface charges. This charged domain supports the interaction with the M1 matrix protein [32].

The structural arrangement of the histidine and tryptophan inside the pore of the AM2 and BM2 suggests that the two residues play an essential role in the channel selectivity and channel gating (Fig. 6.4e). Functional mutagenesis [91] and NMR measurements [92] showed that proton transport across the membrane through the AM2 channel involves cycles of histidine protonation and deprotonation, and that the histidines serve as proton shuttling devices. Not all histidines can be protonated at the same time in the narrow channel, as protonation of one histidine would increase the energy barrier for the protonation of another histidine. Indeed, multiple pKa values (8.2, 6.3 and one below 5.0) have been detected in the AM2 [91, 93]. Therefore, our current understanding of the proton conduction mechanism is that the minimally required unit for pH-dependent proton conduction in the AM2 and BM2 is the His-Trp complex. It was proposed in ref. [93] that in the non-conductive state two pairs of histidines in the tetramer each share one proton, which explains

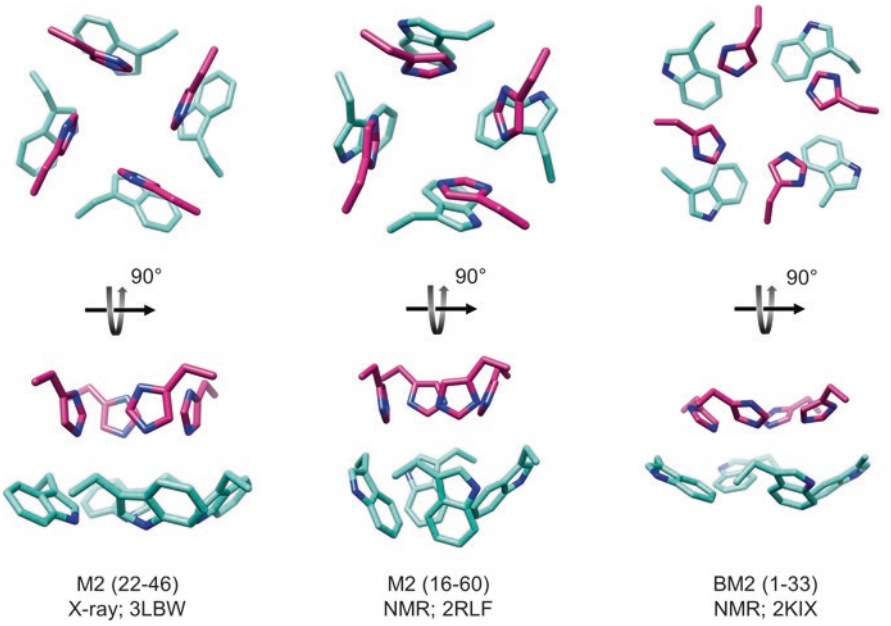

Fig. 6.4b Isolated view of the pore-lining histidine (magenta) and tryptophan (cyan) sidechains in M2 and BM2 channels. Images are from the high resolution crystal structure (3LBW) and NMR structure (2RLF) of M2 and NMR structure of BM2 (2KIX)

the high pK_a ~8.2. Lowering pH results in the protonation of the third histidine from the N-terminal side, which, in turn, disrupts the two histidine dimers and leads to the proton conductive state. It was also proposed that protonation of histidines leads to cation-π interactions between the histidine and tryptophan [94, 95]. The remaining question to be addressed is how does the third protonation affect the tryptophan conformation, allowing proton to be relayed to the C-terminal side of the tryptophan gate [91].

6.3.2 The Funnel Architecture of the p7 Channel

The viroporin p7 encoded by the HCV genome is a 63-residue protein that oligomerizes in membrane to form cation-selective channels [15, 16], with higher selectivity for Ca^{2+} than K^+/Na^+ [96, 97]. The channel activity of p7 is important for the assembly and release of infectious viruses, although the molecular mechanism of this function remains unknown [27, 28]. As in the case of AM2, structural characterization of p7 was confronted with challenges of coping with the hydrophobic and dynamic nature of the protein. Earlier NMR studies of p7 under conditions that support the monomeric state of the protein showed that p7 has three TM helical segments: two in the N-terminal half of the sequence and one near the C-terminus [97,

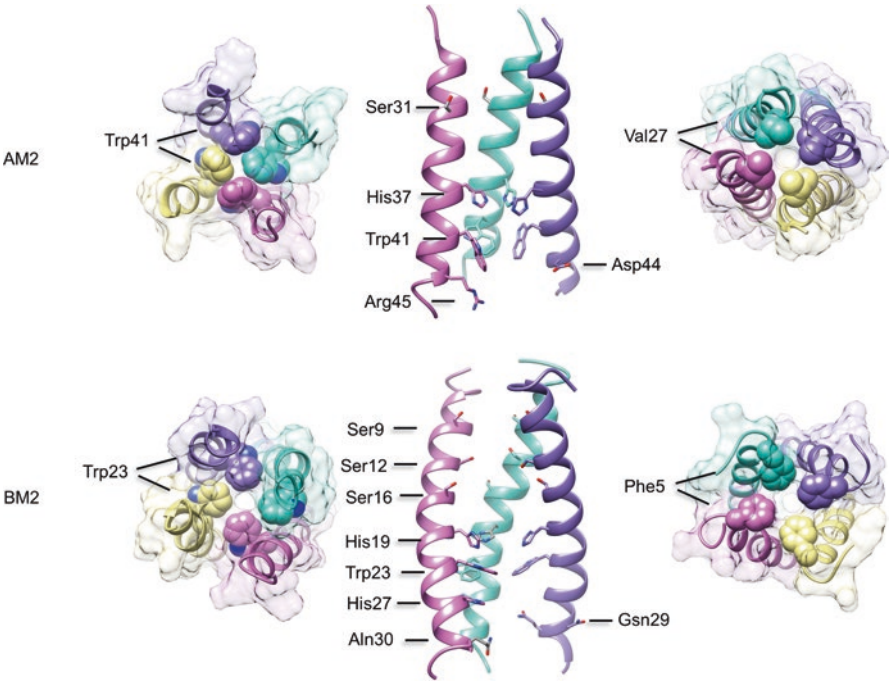

Fig. 6.4c Structural elements of AM2 (top) and BM2 (bottom) important for channel function. C-terminal tryptophan gates of the AM2 (PDB code: 2RLF) and BM2 (PDB code: 2KIX) channels, respectively (Left). The amino acid sidechains important for proton relay, selection, and gating in the TM domains of AM2 and BM2, respectively (Middle). The N-terminal constriction of the AM2 and BM2 channel, respectively (Right)

98]. Although the monomeric state should not conduct ions, it could be involved in interacting with the NS2 protein during virus assembly [33, 34]. The oligomeric form of p7 was first examined using single-particle EM, which showed that p7 from HCV genotype 2a (JFH-1 strain) assembles into hexamers in 1,2-diheptanoyl-*sn*glycero-3-phosphocholine (DH^7PC) micelles and the complex adopts a flower-like shape that does not resemble any of the known ion channel structures in the database [99]. Later, a more detailed structure of the p7 hexamer was determined by solution NMR using p7 from genotype 5a (EUH1480 strain) reconstituted in dodecylphosphocholine (DPC) micelles [60]. Consistent with the flower-shaped EM images, the NMR structure shows a funnel-like architecture with six minimalist chains, each containing three helical segments: H1, H2, and H3. The H1 and H2 form the narrow and wide regions of the funnel-shaped cavity, respectively, and the H3 helices wrap the channel peripheral by interacting with H1 and H2 (Fig. 6.5a). The assembly strategy adopted by p7 differs significantly from those known channels from bacteria and eukaryotes.

Ion channels typically have two essential features: (1) pore elements that support selective ion dehydration; (2) a gate or constriction that prevents non-specific per-

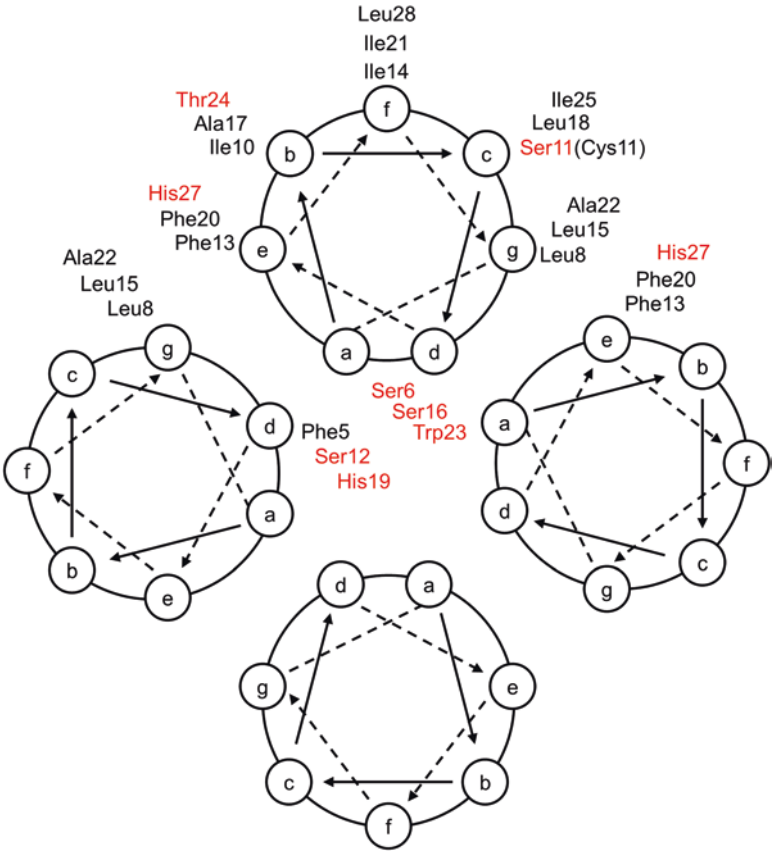

Fig. 6.4d Helical wheel representation of the BM2 [1–33] coiled-coil tetramer. Polar residues are presented in red

meation, but can open in response to regulating factor such as pH, voltage, ligand, or the ion of selection itself [100, 101]. The channel interior of p7 has a number of strongly conserved residues that are likely candidates to serve the above functions. One suspect is Asn9, which forms a ring of carboxamide near the narrow end of the channel (Fig. 6.5b). Residue 9 is asparagine in all strains except being substituted with histidine in genotype 2 viruses. Formation of a ring of carboxylates or carboxamides has been a recurring theme in prokaryotic and eukaryotic channels that have selectivity for divalent cations. For examples, the CorA Mg^{2+} channel has a pentameric ring of asparagines [102], and the calcium release-activated calcium (CRAC) channel Orai has a hexameric ring of aspartic acids [103]. These channels all have strong selectivity for divalent cations, although they can also conduct monovalent cations such as Na^{+} and K^{+}. In addition to the Asn9 ring, residues near the hinge between H1 and H2 (Ser12, Asn16, Trp21) are in an arrangement that may also bind

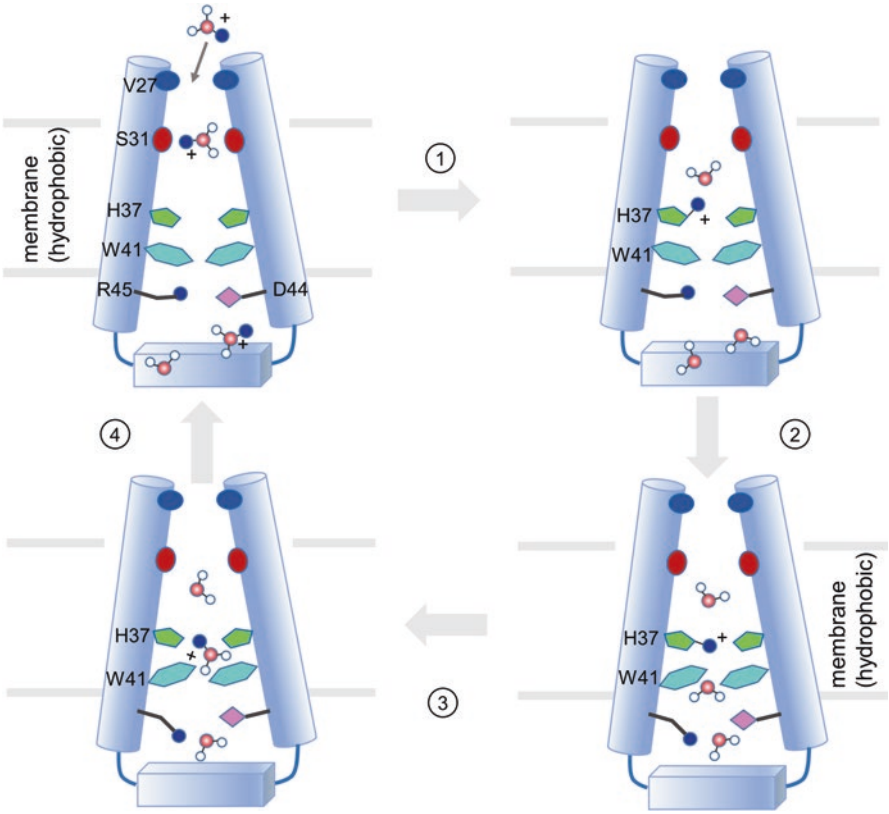

Fig. 6.4e Cartoon of the mechanism of proton conduction. (*1*) Channel breathing allows protons to be relayed cross the Val27 barrier. (*2*) The protons bind to His37 imidazole, and protonation of His37 triggers opening of the Trp41 gate. (*3*) C-terminal water molecules accept protons from protonated His37. (*4*) Polar residues Asp44 and Arg45 facilitate proton exit

cations (Fig. 6.5b), although these residues have not yet been tested in functional assays.

In addition to what appears to be the cation selectivity ring near the narrow, N-terminal exit of the channel, the wider, C-terminal entrance of the channel is decorated with a conserved ring of arginines or lysines (Fig. 6.5b). Placement of a positively charged ring at the entrance was anticipated because it may repel cations. But an earlier study reported that a designed TM barrel with internal arginine-histidine dyads forms efficient cation selective channels [104] because the immobile arginines can recruit mobile anions, which in turn facilitate cations to diffuse through the pore. It is interesting to note that a highly basic region containing Arg155, Lys159 and Lys163 in the pore was also found in the CRAC Orai structure [103]. One possible role of these basic residues in cation selective channels is binding and obstructing anions while allowing cations to diffuse into the pore. This

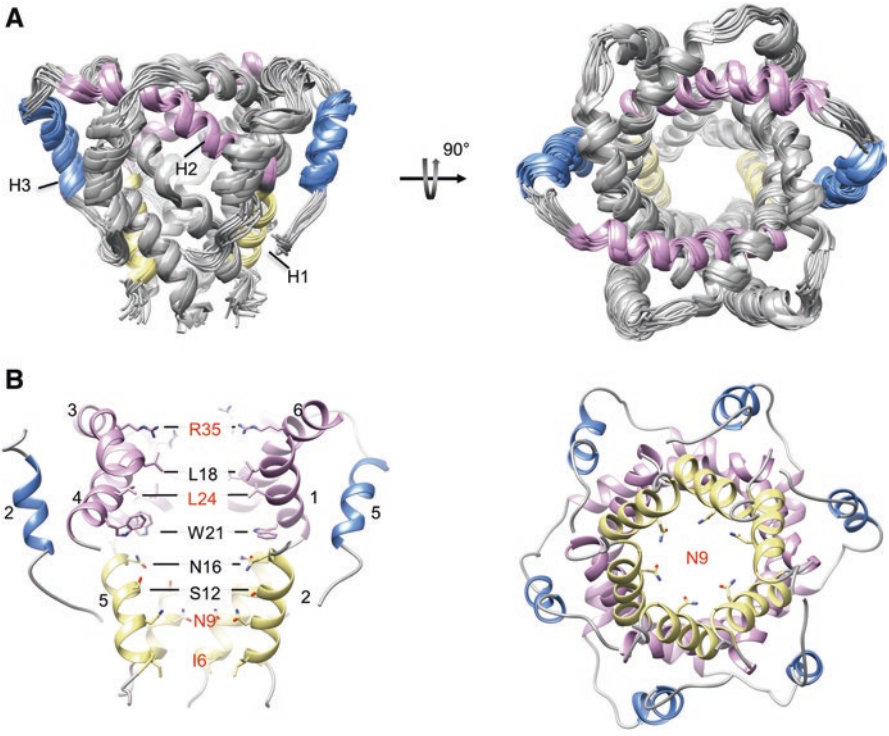

Fig. 6.5 The funnel architecture and pore elements of the p7 channel
(**a**) NMR structure of the p7 hexamer. Left panel: cartoon (cylinder) representation illustrating the funnel architecture of the channel. Right panel: global arrangement of H1, H2 and H3 helical segments in the assembled hexamer, showing that the i and i + 3 monomers form a symmetric pair in the hexamer
(**b**) Pore-lining elements of the p7 channel. Left panel: Cutaway view of the channel showing the pore-lining residues, with residues in red being strongly conserved. The numbers next to the helical segments represent the monomers to which the helices belong. Right panel: the view of the N-terminal opening of the channel showing the carboxamide ring formed with Asn9 sidechains

mechanism would be consistent with the observation that replacing Arg35 with negatively charged aspartic acid largely abrogated conductance [60].

There are still many unanswered questions. Does the NMR structure, solved in the absence of Ca^{2+} and inhibitors, represent the open or closed state of the channel (if the two states exist)? How strong is the Ca^{2+} selectivity of p7? Or was p7 developed as a general, unspecific cation channel for the purpose of dissipating membrane potential? For example, another recently study reported p7 activity in dissipating proton gradients within cell membrane compartments [105]. It is unclear what ion flux mediated by p7 plays a dominant role in the HCV life cycle. From a structural perspective, the funnel-like architecture is formed with multiple helical segments connected by hinges and short loops and we believe this flexibility can afford the dynamic opening and closing of the tip of the channel.

6.3.3 Drug Binding of Viroporins

Probably the most intriguing aspect of small molecule interaction with viroporin is the finding that the adamantane derivatives amantadine and rimantadine have inhibitory effect on multiple viroporins including the influenza AM2 and HCV p7. Amantadine (Symadine) or rimantadine (Flumadine) was the first licensed drug for treating influenza infections [106]. In fact, the compound also played critical roles in the early days of functional characterization of the AM2 channel [107–109]. The BM2 channel is a functional and structural homolog of AM2 but is not sensitive to the adamantane family of drugs [11]. Remarkably, the HCV p7 channel structure is completely different but showed detectable, though not strong, sensitivity to rimantadine [15, 110]. The mechanism of how amantadine/rimantadine inhibit the AM2 channel has been elusive for quite some time. Previous confusion came mainly from the multiple binding sites that have been observed experimentally. In a crystallographic study of the AM2 TMD (residues 24–46) in the presence of amantadine, the drug density was found inside the channel near residue Ser31, but at structural resolution of 3.5 Å, it was difficult to confirm the position of amantadine binding [56]. At the same time, however, a solution NMR study of a longer version of AM2 (residues 18–60) showed that rimantadine binds to an external, lipid-facing pocket around residue Asp44 between adjacent TM helices [62].

The two different binding sites obviously suggest very different mechanisms of inhibition. One is the drug directly blocking the channel passage, and the other is the drug binding to the external site allosterically favors the closed state of the channel. Subsequent solid-state NMR measurements of the AM2 in lipid bilayer showed that both sites exist, with higher affinity for the internal site [87]. The strongest evidence that the internal site is the primary site of drug action came from functional studies using an AM2-BM2 chimera protein [111, 112]. In this study, the authors constructed a chimera of M2 variants from influenza A and B viruses that contains only internal site showed that the chimera channel is still amantadine sensitive, indicating that the internal site is the primary site of drug inhibition. Later, the complex structure of the TMD of the chimera with rimantadine was determined by solution NMR, providing a detailed view of the drug binding inside the channel pore [70]. The drug binding site consists of eight methyl groups of the M2 tetramer (two from each subunit: Val27 $C^{\gamma 1}H_3$ and Ala30 $C^{\beta}H_3$) that form a deep internal hydrophobic pocket surrounding the adamantane cage of the drug (Fig. 6.6a). The structure also shows that the nitrogen of the rimantadine amino group may form a hydrogen bond with the backbone carbonyl oxygen of Ala30 of one of the four subunits. The terminal methyl group of the rimantadine is in the middle of the pore, facing the open space in the channel around the Gly34 position. The structure also shows that rimantadine binding is slightly tilted: its vertical axis is on average ~20° from the C4 symmetry axis of the channel. The tilt angle is consistent with the amantadine tilt in the M2 channel observed with solid-state NMR spectroscopy [87].

In addition to blocking the AM2 channel, the amantadine and its derivatives have also been shown to pose some inhibitory effects on the p7 channel conductance [15,

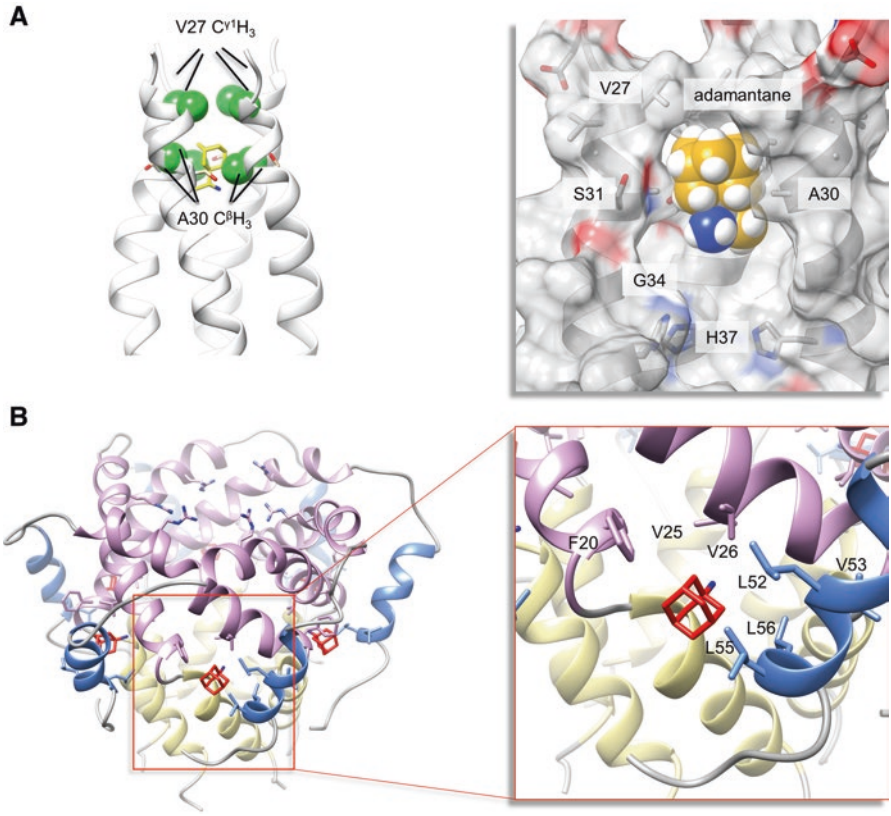

Fig. 6.6 The amantadine and rimantadine binding sites in the M2 and p7 channels
(**a**) The precise NMR structure of the AM2–BM2 chimeric channel with rimantadine determined in DHPC micelles and at pH 7.5. Left panel: detailed illustration of the methyl groups (in green) that interact with the adamantane cage. Right panel: surface representation for showing the hydrophobic pocket that fits the drug snuggly. One of the four subunits is omitted for drug visibility
(**b**) The amantadine or rimantadine binding site of the p7 channel determined by NMR in DPC micelles and at pH 6.5. Left panel: the drug binds to six equivalent hydrophobic pockets of the p7 channel. Right panel: a close view of amantadine docked into the binding pocket as determined using NMR NOE restraints
(c) Comparison between adamantane binding sites of influenza M2 and HCV p7 channels
Top: The internal pocket that wraps around rimantadine in the AM2–BM2 chimeric channel. The AM2–BM2 chimeric channel is a well-behaved model system wth its N-terminal half is from influenza A M2 protein (sensitive to amantadine or rimantadine inhibition) and its C-terminal half is from influenza BM2 protein (insensitive to amantadine or rimantadine). On the right panel, one subunit of the tetrameric complex is removed to unveil the channel interior
Bottom: amantadine binds to the peripheral pockets between the H2 and H3 helices; and a representative pocket among six equivalent pockets in the p7 hexamer

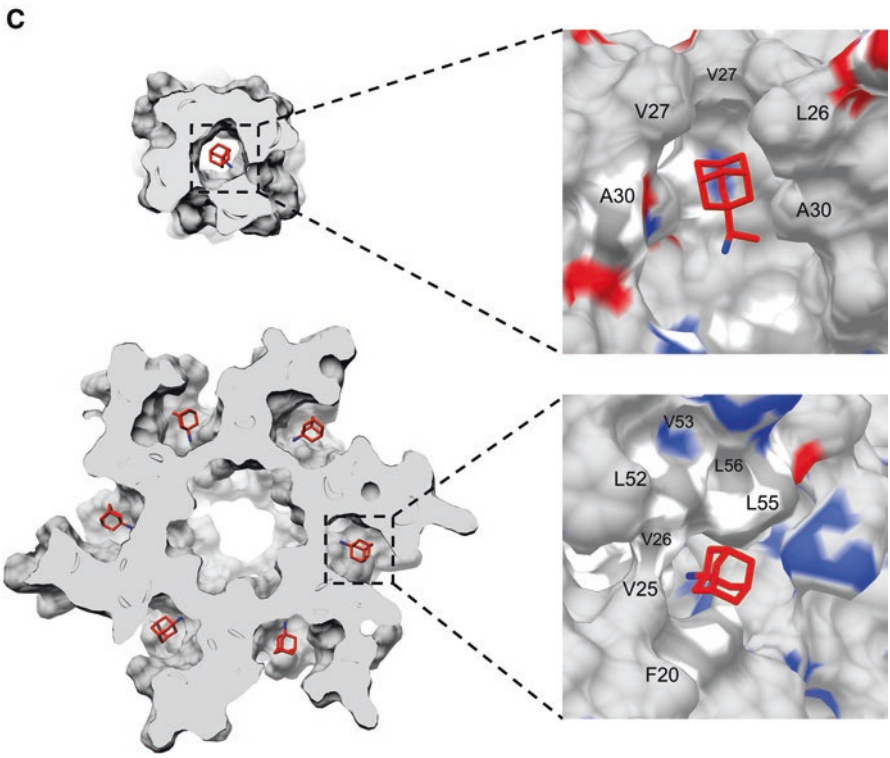

Fig. 6.6 (continued)

113]. The physical binding sites of amantadine and rimantadine have been identified in p7 of genotype 5a using intermolecular NOE experiments [60]. The NOE data revealed that amantadine or rimantadine binds to six equivalent hydrophobic pockets (due to the six-fold symmetry of the p7 channel) between the pore-forming and peripheral helices (Fig. 6.6b). In each site, Leu52, Leu53, and Leu56 from H3 and Val25, Val26, and Phe20 from H2 appear to form a hydrophobic pocket that wraps around the adamantane cage of the drug. The amino group of amantadine or rimantadine is facing the largely hydrophilic channel lumen. An important property of the drug binding site is that it consists of elements from different helical segments and from different monomers. As rationalized above, permeation of cations through the p7 channel may depend on opening the narrow end of the funnel, which in turn depends on the reorientation of the helical segments. The binding of adamantane derivatives to the pocket may inhibit channel activity allosterically by causing the channel to close. Indeed, an NMR relaxation dispersion study showed that residues at the H1-H2 hinge (Phe19) and the narrow end of the cavity (Val7, Leu8) experienced substantial chemical exchanges (k_{ex}~1000 ± 79 s^{-1} and ~10% excited state). This data is consistent with movements of the H1 helices that cause the tip of the funnel to open and close. More importantly, addition of rimantadine slowed down motion at the tip of the channel, as relaxation dispersion curve for Val7, which has

significant chemical exchange in the apo state, is completely flat in the drug-bound state [114]. The dispersion curve of Phe19 is also significantly flatter, and individual curve fit yielded k_{ex} value of 67 ± 182 s^{-1}. Clearly, rimantadine binding makes the channel less dynamic. Therefore, the rimantadine may thus act as a "molecular wedge" that prevents the dynamic "breathing" of the channel required for ion conduction.

Comparing the amantadine or rimantadine binding mode of HCV p7 to that of influenza AM2 shows two fundamentally different mechanisms of drug inhibition. In the case of AM2, one drug binds to one channel. Drug binding inhibits proton transport by directly blocking the channel passage; it also prevents channel from opening. In the case of p7, amantadine and rimantadine are clearly too small to block the channel. They instead bind to six equivalent sites outside of the channel cavity, which can afford up to six drugs per channel. If rimantadine binding to this site is relevant to inhibition, as crudely suggested by previous functional mutagenesis, drug binding to these sites inhibits cation conduction with an allosteric mechanism, possibly by stabilizing the closed state of the channel.

Although the mechanisms of drug inhibition may be completely different, the structural bases that govern drug-binding affinity for AM2 and p7 are actually similar, and they involve hydrophobicity and size of the pocket, and position of the drug amino group (Fig. 6.6c). In the case of the AM2 tetramer, the drug adamantane cage fits snuggly in a hydrophobic pocket formed by eight methyl groups from Val27 and Ala30 (two from each subunit), while the drug amino group forms polar contact with the backbone oxygen of Ala30 and points to the polar region of the channel cavity. For the p7 channel, the adamantane cage is in contact with ten methyl groups and an aromatic group from the protein. These hydrophobic groups form a deep hydrophobic pocket that also matches closely the size of the adamantane cage. The amino group of amantadine or rimantadine points to the channel lumen; it is in position to form polar contacts with the electronegative groups such as backbone carbonyl of residues 15–17. Hence, having a greasy pocket for the adamantane cage and a nearby electronegative group to interact with the amino group may be a general requirement for amantadine or rimantadine binding.

6.4 The Transmembrane Domains of Viral Fusion Proteins

Previous functional mutagenesis studies have suggested that the TMDs of viral fusion proteins are not only limited to the function of membrane anchoring, but also involved in other functions such as membrane fusion or assembly of the fusion protein on the viral membrane. For example, sequence analysis of the HA from mutant viruses and site-specific mutagenesis of the fusion peptide identified a group of mutations in the N-terminal half of the influenza HA TMD severely affected membrane fusion (the hemifusion to pore formation) [115–117]. In the case of HIV-1, multiple lines of evidences suggest that the TMD of gp41 is not merely a membrane anchor, but plays critical roles in membrane fusion and viral infectivity [118–122].

The amino acid sequence of gp41 TMD is also highly interesting. There is a Gly rich motif in the TMD, which suggests some sort of oligomerization. Even more peculiar is the presence of a conserved arginine in the middle of the predicted TM region. Unlike the structural biology of viroporins, there is essentially no structural information of TMDs of viral fusion proteins except for that of the TMD of HIV-1 Env. Hence, we focus on the discussion on the trimeric membrane anchor of the TMD of the HIV-1 envelope spike.

6.4.1 HIV-1 Envelope Glycoprotein

HIV-1 envelope spike [Env; trimeric $(gp160)_3$, cleaved to $(gp120/gp41)_3$] is a type I membrane protein that fuses viral and host cell membranes to initiate viral infection [123]. The gp120 and gp41 are the receptor recognition and membrane fusion proteins, respectively. Conformational changes in gp120 when triggered by binding to receptor (CD4) and co-receptor (e.g., CCR5 or CXCR4) lead to a cascade of refolding events in gp41 (similar to those illustrated in Fig. 6.2a), and ultimately to membrane fusion [39, 124–126]. The mature and functional Env spikes, $(gp120/gp41)_3$, are the sole antigens on the virion surface and thus important candidates for vaccine development [127, 128]. The native prefusion conformation of HIV-1 Env is recognized by most broadly neutralizing antibodies (bnAbs) [129–131] and it is generally believed to have the potential to induce such antibody responses. Thus, the native conformation of Env spikes on the surface of virions is extremely important to immunogen design in B-cell based vaccine development.

A vast amount of structures of the ectodomain (ECD) of the gp120/gp41 complex have been determined [39, 124, 125, 132–139], but relatively little is known about the TM and membrane proximal regions of gp41 due to challenges of preserving the native-like folding of these regions in membrane mimetic media. It has been shown that truncations in the cytoplasmic tail (CT) of gp41 could alter the antigenic surface of the Env ECD on the opposite side of the membrane [129], suggesting that the ECD, the TMD, and the membrane proximal regions are conformationally coupled, and thus the conformational stability of the TMD is an important consideration for immunogen design in B-cell based HIV-1 vaccine development. Recently, the NMR structure of the gp41 TMD has been solved in bicelles (made of DMPC lipid and DHPC detergent; $q = 0.5$) [68] using a gp41 fragment (residues 677–716) from a clade D HIV-1 isolate 92UG024.2, designated $gp41^{HIV1D}(677–716)$. The TMD forms a well-structured trimer, almost helical all the way from the N- to the C-terminal end. It shows two peculiar features not seen with other known oligomeric TM helices (TMHs) (Fig. 6.7a).

One unusual feature is that the TMD trimer appears to be stabilized by two separate packing modes (Fig. 6.7c). The N-terminal half encompassing the GxxxG motif forms a coiled-coil trimer, whereas the C-terminal half is held together by a network of polar contacts, which we named the hydrophilic core. For the N-terminal coiled-coil, the helical wheel representation of the trimer clearly indicates packing of

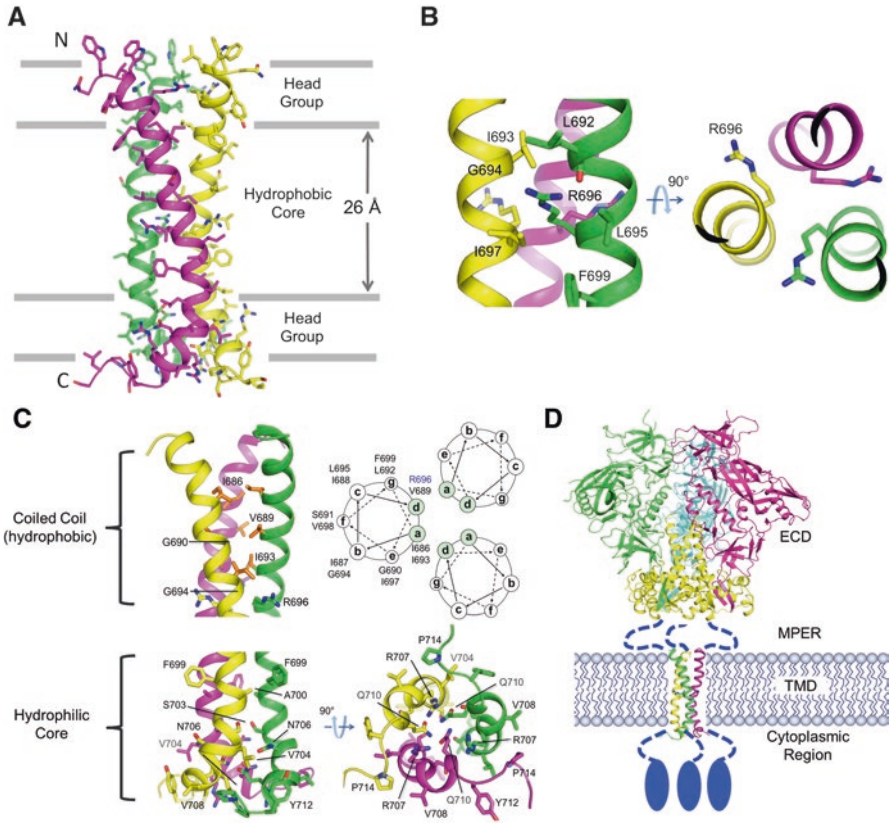

Fig. 6.7 NMR structure of the TMD of HIV-1 gp41 in bicelles
(**a**) Ribbon representation of the gp41 TMD trimer. The protein construct used for structure determination is from HIV-1 clade D (residues 677–716). The bicelles are formed with 1,2- Dimyristoyl-*sn*-Glycero-3-Phosphocholine (DMPC) and 1,2-Dihexanoyl-*sn*-Glycero-3- Phosphocholine (DHPC) at DMPC/DHPC molar ratio 0.5. The approximate placement of the trimer structure in the presumed DMPC bilayer was based on the solvent paramagnetic relaxation enhancement of the four arginines (R683, R696, R707, and R709) (Ref. [68])
(**b**) Zoomed view of the R696 at the middle of the TM helix
(**c**) The N-terminal half of the structure with hydrophobic residues (orange) (top left) arranged in the coiled-coil pattern (top right). Bottom: The C-terminal half of the structure showing an array of polar residues that form the C-terminal hydrophilic core. The network of polar contacts is hypothesized to stabilize the trimer
(**d**) Illustration showing that the conformation of the MPER and the cytoplasmic tail attached to the TMD trimer in a lipid bilayer environment are still missing

hydrophobic residues such as Ile and Val at the "a" and "d" positions of the heptad motif, forming a hydrophobic core. The GxxxG is a well-known motif that drives TMH dimerization [58, 140, 141]. In the classic example of the glycophorin A TMD dimer structure, the two glycines of one TMH allow close packing with the GxxxG face of another TMH, resulting in a very strong TMH dimeric complex [58, 140].

There has been no previous report, however, of the GxxxG involvement in TMH trimerization. In the coiled-coil region of the HIV-1 Env TMD, only G690 is involved in the trimer assembly, i.e., its small sidechain allows a close VDW contact with V689 of the adjacent TMH. The other glycine, G694, is on the periphery of the trimer facing outwards and its mutation to alanine or valine has essentially no effect on TMD trimerization, as well as Env functions [68]. Therefore, the key difference in the structural role of the GxxxG motif between the glycophorin A TMD dimer and HIV-1 Env TMD trimer is that both the glycines are required for forming inter-monomer contacts in the dimer, while only one glycine is important for the trimeric assembly.

TM segments of many viral fusion proteins contain a GxxxG motif or "SmallxxxSmall" motifs ("Small" refers to residues with a small side chain, such as, glycine, alanine, serine or cysteine) [142–144], suggesting that oligomerization of their TMDs may be a common property. For example, recent biochemical evidence has shown that the TMDs of hepatitis C virus envelope glycoproteins E1 and E2 form stable dimers or trimers that are also resistant to SDS [143]. No high-resolution structure of any TMD oligomer from other viral fusion proteins has been reported, due to technical challenges for structural studies of such constructs in the context of lipid bilayer. The NMR structure of the HIV-1 Env TMD may provide some clues for how other viral fusion proteins oligomerize in the membrane.

Another peculiar feature is the presence of three copies of arginine (R696) near the middle of the TMHs (Fig. 6.7b), suggesting three unbalanced charges in the hydrophobic core of the membrane if the Arg remains protonated. In the NMR structure, the tips of the long sidechains of these arginines are facing lipids and each of them is surrounded by three hydrophobic residues (L692, L695, and I697). It is also interesting to note that R696 occupies a "d" position in the coiled-coil, with its Cβ facing inwards to the trimer interface. Precise physical basis of how R696 is accommodated in the highly hydrophobic environment remains unclear, but the underlying mechanism must tolerate a Lys residue, which is present in some viral isolates at this position. It is interesting to mention that the NOE experiment for the R696 epsilon protons showed clear water NOE even with a short NOE mixing time of 60 ms, suggesting that the Arg is somehow hydrated in the membrane.

A positively-charged Arg or Lys in the TM segment of viral fusion protein is present in some related enveloped viruses, including simian immunodeficiency virus, caprine arthritis and encephalitis virus, equine infectious anemia virus, visna virus, and foamy virus, as well as in hepatitis C virus [145–150], but absent in many others. It is therefore not a prerequisite for viral membrane fusion in general [121]. Functional mutagenesis indicated that the R696A mutant of HIV-1 Env showed some defect in cell-cell fusion, but it could be fully compensated by high Env expression [68]. Moreover, this mutant has wildtype viral infectivity. In vitro infectivity and cell-cell fusion do not, however, mimic all the conditions under which the virus moves from one cell to another in an infected individual, nor are those assays particularly sensitive to physiologically relevant kinetic parameters.

6.5 Future Perspective

The structures of viroporins discussed above are all substantially different from any of the channel structures found in prokaryotes and eukaryotes, and are thus clean structural targets for developing antiviral compounds. The available structures also suggest that viroporins generally adopt minimalist architecture and can possess structural features compatible with selective ion transport. The viral channels, however, may not be as functionally robust or specifically regulated as some of their counterparts in prokayrotes and eukaryotes, because viruses often do not need intricate regulation of channel activities during their infection cycles. Having minimalist structure also makes viroporins fragile and sensitive to the membrane environment. This is reflected by the conformational variations observed for the AM2 channel in different reconstitution media. Therefore, it remains important to examine these viroporins in more native environments, e.g., lipid bilayer and full-length proteins. As solid-state NMR continues to improve spectral resolution [87, 89], obtaining detailed structures of viroporins in liposomes should in principle be feasible in the near future. Alternatively, the ideal bicelle system can be explored with solution NMR to revisit some of the viroporin structures determined previously in detergent micelles. Future establishment of the NMR systems for viroporins under more native conditions would certainly provide versatile and effective platforms for investigating inhibitor binding.

Apart from the progress in structure determination, major challenges lie ahead in the functional aspects of viroporin research. The precise functional roles of many viroporins are still unclear. Moreover, due to the lack of robust single-channel recording setups suitable for viroporins, the ion conductance properties of most viroporins have not been fully characterized. Therefore, better definition of the functional roles and channel properties of viroporins will certainly draw greater enthusiasm for developing therapeutics that target this interesting family of membrane channels.

The example from HIV-1 Env suggests that TMDs of viral fusion proteins can adopt very interesting structures, and the distinct structural features certainly allude to their roles in viral fusion protein assembly and incorporation into the envelope, as well as in the process of membrane fusion. The NMR structural study of the HIV-1 gp41 TMD in bicelles with $q = 0.5$ [68] demonstrates that the structures of most of the viral fusion protein TMDs can in principle be determined in essentially lipid bilayer environment using modern NMR techniques. Moreover, the combined use of ideal bicelles ($q \geq 0.5$) and solvent paramagnetic relaxation enhancement measurements can be used to determine the membrane partition of the TMDs in the bilayer region of the bicelles [63]. We believe the next major challenge lies in understanding the roles of the fusion protein TMDs in the fusion mechanism. In the cases of the flu HA and HIV gp41, for example, new experiments need to be designed to address questions such as, “Does the TMD interact with the fusion domain in the hemifusion stage in which the two domains are presumably in close proximity?”

and “Does the TMD play a role in facilitating the conversion from the hemifusion to the pore formation?”

Understanding the structural properties and conformational stability of the TMD may also have far reaching implication to vaccine development and this has been recognized at least for HIV-1. As mentioned above, truncations in the CT of the Env could drastically alter the sensitivity of the Env ECD to the known trimer-specific bnAbs [129]. The continuous structure from the N- to C- terminal ends of the Env TMD, as observed by NMR, suggests that the Env ECD can be structurally coupled via the TMD. Indeed, it has also been shown that the Env TMD can also modulate the antigenic structure of the ECD in a cell-cell fusion assay and a pseudovirus-based neutralization assay [68]. The results show direct correlation that more disrupted TMD trimer led to less inhibition or neutralization by the trimer-specific bnAbs that target only the ECD. The results suggest that the stability of the TMD trimer is an important consideration when designing immunogens for HIV vaccines.

The HIV Env TMD is, however, not directly linked to the Env ECD. Another important segment known as the membrane-proximal external region (MPER) is the direct link that connects the TMD to the ECD, and thus it could in principle also affect the antigenic properties of the Env ECD. The MPER sequence is extremely conserved with five absolutely conserved tryptophans, suggesting that the MPER probably also has interesting structural features. The conformation of the MPER attached to the TMD trimer in a lipid bilayer environment is still unknown (Fig. 6.7d). Previous NMR studies of an isolated MPER peptide in detergent micelle suggested that the MPER is monomeric and folds into a kinked helix with many hydrophobic residues embedded in the micelles [151, 152]. This of course would have a rather negative implication for the MPER as a vaccine epitope because antibodies that bind to the MPER must dig it out of the lipids, which could be accompanied with polyreactivities. The Env TMD appears to be well structured and assembled strongly to trimers. Hence, the structure of the MPER when connected to the trimeric TMD and in the context of a lipid bilayer remains to be characterized.

References

1. Madan V, et al. Plasma membrane-porating domain in poliovirus 2B protein. A short peptide mimics viroporin activity. J Mol Biol. 2007;374(4):951–64.
2. Madan V, Redondo N, Carrasco L. Cell permeabilization by poliovirus 2B viroporin triggers bystander permeabilization in neighbouring cells through a mechanism involving gap junctions. Cell Microbiol. 2010;12(8):1144–57.
3. Agirre A, Lorizate M, Nir S, Nieva JL. Poliovirus 2b insertion into lipid monolayers and pore formation in vesicles modulated by anionic phospholipids. Biochim Biophys Acta. 2008;1778(11):2621–6.
4. Melton JV, et al. Alphavirus 6K proteins form ion channels. J Biol Chem. 2002;277(49):46923–31.
5. Sanz MA, Perez L, Carrasco L. Semliki Forest virus 6K protein modifies membrane permeability after inducible expression in Escherichia coli cells. J Biol Chem. 1994;269(16):12106–10.

6. Firth AE, Chung BY, Fleeton MN, Atkins JF. Discovery of frameshifting in Alphavirus 6K resolves a 20-year enigma. Virol J. 2008;5:108.
7. Antoine AF, et al. The alphavirus 6K protein activates endogenous ionic conductances when expressed in Xenopus oocytes. J Membr Biol. 2007;215(1):37–48.
8. Pielak RM, Chou JJ. Influenza M2 proton channels. Biochim Biophys Acta. 2011;1808(2):522–9.
9. Wang J, Qiu JX, Soto C, DeGrado WF. Structural and dynamic mechanisms for the function and inhibition of the M2 proton channel from influenza A virus. Curr Opin Struct Biol. 2011;21(1):68–80.
10. Cross TA, Dong H, Sharma M, Busath DD, Zhou HX. M2 protein from influenza A: from multiple structures to biophysical and functional insights. Curr Opin Virol. 2012;2(2):128–33.
11. Mould JA, et al. Influenza B virus BM2 protein has ion channel activity that conducts protons across membranes. Dev Cell. 2003;5(1):175–84.
12. Schubert U, et al. Identification of an ion channel activity of the Vpu transmembrane domain and its involvement in the regulation of virus release from HIV-1-infected cells. FEBS Lett. 1996;398(1):12–8.
13. Marassi FM, et al. Correlation of the structural and functional domains in the membrane protein Vpu from HIV-1. Proc Natl Acad Sci U S A. 1999;96(25):14336–41.
14. Romer W, et al. Channel activity of a viral transmembrane peptide in micro-BLMs: Vpu(1-32) from HIV-1. J Am Chem Soc. 2004;126(49):16267–74.
15. Griffin SD, et al. The p7 protein of hepatitis C virus forms an ion channel that is blocked by the antiviral drug, Amantadine. FEBS Lett. 2003;535(1–3):34–8.
16. Pavlovic D, et al. The hepatitis C virus p7 protein forms an ion channel that is inhibited by long-alkyl-chain iminosugar derivatives. Proc Natl Acad Sci U S A. 2003;100(10):6104–8.
17. Xie S, et al. DIDS blocks a chloride-dependent current that is mediated by the 2B protein of enterovirus 71. Cell Res. 2011;21(8):1271–5.
18. Plugge B, et al. A potassium channel protein encoded by chlorella virus PBCV-1. Science. 2000;287(5458):1641–4.
19. Gazzarrini S, et al. The viral potassium channel Kcv: structural and functional features. FEBS Lett. 2003;552(1):12–6.
20. Strauss M, Levy HC, Bostina M, Filman DJ, Hogle JM. RNA transfer from poliovirus 135S particles across membranes is mediated by long umbilical connectors. J Virol. 2013;87(7):3903–14.
21. Panjwani A, et al. Capsid protein VP4 of human rhinovirus induces membrane permeability by the formation of a size-selective multimeric pore. PLoS Pathog. 2014;10(8):e1004294.
22. Martin K, Helenius A. Nuclear transport of influenza virus ribonucleoproteins: the viral matrix protein (M1) promotes export and inhibits import. Cell. 1991;67(1):117–30.
23. Helenius A. Unpacking the incoming influenza virus. Cell. 1992;69(4):577–8.
24. Grambas S, Bennett MS, Hay AJ. Influence of amantadine resistance mutations on the pH regulatory function of the M2 protein of influenza A viruses. Virology. 1992;191(2):541–9.
25. Nieva JL, Madan V, Carrasco L. Viroporins: structure and biological functions. Nat Rev Microbiol. 2012;10(8):563–74.
26. Agarkova I, et al. Chlorovirus-mediated membrane depolarization of Chlorella alters secondary active transport of solutes. J Virol. 2008;82(24):12181–90.
27. Jones CT, Murray CL, Eastman DK, Tassello J, Rice CM. Hepatitis C virus p7 and NS2 proteins are essential for production of infectious virus. J Virol. 2007;81(16):8374–83.
28. Steinmann E, et al. Hepatitis C virus p7 protein is crucial for assembly and release of infectious virions. PLoS Pathog. 2007;3(7):e103.
29. Madan V, Castello A, Carrasco L. Viroporins from RNA viruses induce caspase-dependent apoptosis. Cell Microbiol. 2008;10(2):437–51.
30. Chen BJ, Leser GP, Jackson D, Lamb RA. The influenza virus M2 protein cytoplasmic tail interacts with the M1 protein and influences virus assembly at the site of virus budding. J Virol. 2008;82(20):10059–70.

31. Imai M, Kawasaki K, Odagiri T. Cytoplasmic domain of influenza B virus BM2 protein plays critical roles in production of infectious virus. J Virol. 2008;82(2):728–39.
32. Wang J, Pielak RM, McClintock MA, Chou JJ. Solution structure and functional analysis of the influenza B proton channel. Nat Struct Mol Biol. 2009;16(12):1267–71.
33. Gouklani H, et al. Identification of specific regions in hepatitis C virus core, NS2 and NS5A that genetically interact with p7 and co-ordinate infectious virus production. J Viral Hepat. 2013;20(4):e66–71.
34. Vieyres G, et al. Subcellular localization and function of an epitope-tagged p7 viroporin in hepatitis C virus-producing cells. J Virol. 2013;87(3):1664–78.
35. Harrison SC. Mechanism of membrane fusion by viral envelope proteins. Adv Virus Res. 2005;64:231–61.
36. White JM, Delos SE, Brecher M, Schornberg K. Structures and mechanisms of viral membrane fusion proteins: multiple variations on a common theme. Crit Rev Biochem Mol Biol. 2008;43(3):189–219.
37. Bullough PA, Hughson FM, Skehel JJ, Wiley DC. Structure of influenza haemagglutinin at the pH of membrane fusion. Nature. 1994;371(6492):37–43.
38. Checkley MA, Luttge BG, Freed EO. HIV-1 envelope glycoprotein biosynthesis, trafficking, and incorporation. J Mol Biol. 2011;410(4):582–608.
39. Chan DC, Fass D, Berger JM, Kim PS. Core structure of gp41 from the HIV envelope glycoprotein. Cell. 1997;89(2):263–73.
40. Harrison SC. Mechanism of membrane fusion by viral envelope proteins. Adv Virus Res. 2005;64:231–59.
41. Wang W, DeFeo CJ, Alvarado-Facundo E, Vassell R, Weiss CD. Intermonomer interactions in hemagglutinin subunits HA1 and HA2 affecting hemagglutinin stability and influenza virus infectivity. J Virol. 2015;89(20):10602–11.
42. Kielian M. Class II virus membrane fusion proteins. Virology. 2006;344(1):38–47.
43. Modis Y. Class II fusion proteins. Adv Exp Med Biol. 2013;790:150–66.
44. Modis Y, Ogata S, Clements D, Harrison SC. Structure of the dengue virus envelope protein after membrane fusion. Nature. 2004;427(6972):313–9.
45. Nayak V, et al. Crystal structure of dengue virus type 1 envelope protein in the postfusion conformation and its implications for membrane fusion. J Virol. 2009;83(9):4338–44.
46. Stiasny K, Bressanelli S, Lepault J, Rey FA, Heinz FX. Characterization of a membrane-associated trimeric low-pH-induced form of the class II viral fusion protein E from tick-borne encephalitis virus and its crystallization. J Virol. 2004;78(6):3178–83.
47. Backovic M, Jardetzky TS. Class III viral membrane fusion proteins. Adv Exp Med Biol. 2011;714:91–101.
48. Backovic M, Leser GP, Lamb RA, Longnecker R, Jardetzky TS. Characterization of EBV gB indicates properties of both class I and class II viral fusion proteins. Virology. 2007;368(1):102–13.
49. Backovic M, Jardetzky TS. Class III viral membrane fusion proteins. Curr Opin Struct Biol. 2009;19(2):189–96.
50. Kadam RU, Wilson IA. Structural basis of influenza virus fusion inhibition by the antiviral drug Arbidol. Proc Natl Acad Sci U S A. 2017;114(2):206–14.
51. Blaising J, Polyak SJ, Pecheur EI. Arbidol as a broad-spectrum antiviral: an update. Antivir Res. 2014;107:84–94.
52. Zhu X, et al. Improved pharmacological and structural properties of HIV fusion inhibitor AP3 over Enfuvirtide: highlighting advantages of artificial peptide strategy. Sci Rep. 2015;5:13028.
53. Matthews T, et al. Enfuvirtide: the first therapy to inhibit the entry of HIV-1 into host CD4 lymphocytes. Nat Rev Drug Discov. 2004;3(3):215–25.
54. Haynes BF, Kelsoe G, Harrison SC, Kepler TB. B-cell-lineage immunogen design in vaccine development with HIV-1 as a case study. Nat Biotechnol. 2012;30(5):423–33.

55. Haynes BF, Moody MA, Liao HX, Verkoczy L, Tomaras GD. B cell responses to HIV-1 infection and vaccination: pathways to preventing infection. Trends Mol Med. 2011;17(2):108–16.
56. Stouffer AL, et al. Structural basis for the function and inhibition of an influenza virus proton channel. Nature. 2008;451(7178):596–9.
57. Acharya R, et al. Structure and mechanism of proton transport through the transmembrane tetrameric M2 protein bundle of the influenza A virus. Proc Natl Acad Sci U S A. 2010;107(34):15075–80.
58. Trenker R, Call ME, Call MJ. Crystal structure of the glycophorin A transmembrane dimer in lipidic cubic phase. J Am Chem Soc. 2015;137(50):15676–9.
59. Lee JH, Ozorowski G, Ward AB. Cryo-EM structure of a native, fully glycosylated, cleaved HIV-1 envelope trimer. Science. 2016;351(6277):1043–8.
60. OuYang B, et al. Unusual architecture of the p7 channel from hepatitis C virus. Nature. 2013;498(7455):521–5.
61. Call ME, Wucherpfennig KW, Chou JJ. The structural basis for intramembrane assembly of an activating immunoreceptor complex. Nat Immunol. 2010;11(11):1023–9.
62. Schnell JR, Chou JJ. Structure and mechanism of the M2 proton channel of influenza A virus. Nature. 2008;451(7178):591–5.
63. Piai A, Fu Q, Dev J, Chou JJ. Optimal bicelle size q for solution NMR studies of the protein transmembrane partition. Chemistry. 2017;23(6):1361–7.
64. Glover KJ, et al. Structural evaluation of phospholipid bicelles for solution-state studies of membrane-associated biomolecules. Biophys J. 2001;81(4):2163–71.
65. Sanders CR II, Schwonek JP. Characterization of magnetically orientable bilayers in mixtures of dihexanoylphosphatidylcholine and dimyristoylphosphatidylcholine by solid-state NMR. Biochemistry. 1992;31(37):8898–905.
66. Sanders CR, Hare BJ, Howard KP, Prestegard JH. Magnetically-oriented phospholipid micelles as a tool for the study of membrane-associated molecules. Prog Nucl Magn Reson Spectrosc. 1994;26:421–44.
67. Fu Q, et al. Structural basis and functional role of intramembrane Trimerization of the Fas/CD95 death receptor. Mol Cell. 2016;61(4):602–13.
68. Dev J, et al. Structural basis for membrane anchoring of HIV-1 envelope spike. Science. 2016;353(6295):172–5.
69. Oxenoid K, Chou JJ. The structure of phospholamban pentamer reveals a channel-like architecture in membranes. Proc Natl Acad Sci U S A. 2005;102(31):10870–5.
70. Pielak RM, Oxenoid K, Chou JJ. Structural investigation of rimantadine inhibition of the AM2-BM2 chimera channel of influenza viruses. Structure. 2011;19(11):1655–63.
71. Zhao L, et al. Structural basis of interaction between the hepatitis C virus p7 channel and its blocker hexamethylene amiloride. Protein Cell. 2016;7(4):300–4.
72. Lamb RA, Zebedee SL, Richardson CD. Influenza virus M2 protein is an integral membrane protein expressed on the infected-cell surface. Cell. 1985;40(3):627–33.
73. Sugrue RJ, Hay AJ. Structural characteristics of the M2 protein of influenza A viruses: evidence that it forms a tetrameric channel. Virology. 1991;180(2):617–24.
74. Holsinger LJ, Lamb RA. Influenza virus M2 integral membrane protein is a homotetramer stabilized by formation of disulfide bonds. Virology. 1991;183(1):32–43.
75. Paterson RG, Takeda M, Ohigashi Y, Pinto LH, Lamb RA. Influenza B virus BM2 protein is an oligomeric integral membrane protein expressed at the cell surface. Virology. 2003;306(1):7–17.
76. Pinto LH, Lamb RA. The M2 proton channels of influenza A and B viruses. J Biol Chem. 2006;281(14):8997–9000.
77. Neirynck S, et al. A universal influenza a vaccine based on the extracellular domain of the M2 protein. Nat Med. 1999;5(10):1157–63.
78. Jegerlehner A, Schmitz N, Storni T, Bachmann MF. Influenza A vaccine based on the extracellular domain of M2: weak protection mediated via antibody-dependent NK cell activity. J Immunol. 2004;172(9):5598–605.

79. De Filette M, et al. An influenza A vaccine based on tetrameric ectodomain of matrix protein 2. J Biol Chem. 2008;283(17):11382–7.
80. Wang BZ, et al. Enhanced influenza virus-like particle vaccines containing the extracellular domain of matrix protein 2 and a Toll-like receptor ligand. Clin Vaccine Immunol CVI. 2012;19(8):1119–25.
81. Kim EH, et al. Prokaryote-expressed M2e protein improves H9N2 influenza vaccine efficacy and protection against lethal influenza A virus in mice. Virol J. 2013;10:104.
82. Williams JK, Tietze D, Lee M, Wang J, Hong M. Solid-state NMR investigation of the conformation, proton conduction, and hydration of the influenza B virus M2 transmembrane proton channel. J Am Chem Soc. 2016;138(26):8143–55.
83. McCown MF, Pekosz A. Distinct domains of the influenza a virus M2 protein cytoplasmic tail mediate binding to the M1 protein and facilitate infectious virus production. J Virol. 2006;80(16):8178–89.
84. Imai M, Watanabe S, Ninomiya A, Obuchi M, Odagiri T. Influenza B virus BM2 protein is a crucial component for incorporation of viral ribonucleoprotein complex into virions during virus assembly. J Virol. 2004;78(20):11007–15.
85. Pielak RM, Schnell JR, Chou JJ. Mechanism of drug inhibition and drug resistance of influenza A M2 channel. Proc Natl Acad Sci U S A. 2009;106(18):7379–84.
86. Pielak RM, Chou JJ. Solution NMR structure of the V27A drug resistant mutant of influenza A M2 channel. Biochem Biophys Res Commun. 2010;401(1):58–63.
87. Cady SD, et al. Structure of the amantadine binding site of influenza M2 proton channels in lipid bilayers. Nature. 2010;463(7281):689–92.
88. Sharma M, et al. Insight into the mechanism of the influenza A proton channel from a structure in a lipid bilayer. Science. 2010;330(6003):509–12.
89. Andreas LB, et al. Structure and mechanism of the influenza A M218-60 dimer of dimers. J Am Chem Soc. 2015;137(47):14877–86.
90. Harbury PB, Zhang T, Kim PS, Alber T. A switch between two-, three-, and four-stranded coiled coils in GCN4 leucine zipper mutants. Science. 1993;262(5138):1401–7.
91. Pielak RM, Chou JJ. Kinetic analysis of the M2 proton conduction of the influenza virus. J Am Chem Soc. 2010;132(50):17695–7.
92. Hu F, Luo W, Hong M. Mechanisms of proton conduction and gating in influenza M2 proton channels from solid-state NMR. Science. 2010;330(6003):505–8.
93. Hu J, et al. Histidines, heart of the hydrogen ion channel from influenza A virus: toward an understanding of conductance and proton selectivity. Proc Natl Acad Sci U S A. 2006;103(18):6865–70.
94. Betakova T, Hay AJ. Comparison of the activities of BM2 protein and its H19 and W23 mutants of influenza B virus with activities of M2 protein and its H37 and W41 mutants of influenza A virus. Arch Virol. 2009;154(10):1619–24.
95. Otomo K, Toyama A, Miura T, Takeuchi H. Interactions between histidine and tryptophan residues in the BM2 proton channel from influenza B virus. J Biochem. 2009;145(4):543–54.
96. Premkumar A, Wilson L, Ewart GD, Gage PW. Cation-selective ion channels formed by p7 of hepatitis C virus are blocked by hexamethylene amiloride. FEBS Lett. 2004;557(1–3):99–103.
97. Montserret R, et al. NMR structure and ion channel activity of the p7 protein from hepatitis C virus. J Biol Chem. 2010;285(41):31446–61.
98. Cook GA, Opella SJ. Secondary structure, dynamics, and architecture of the p7 membrane protein from hepatitis C virus by NMR spectroscopy. Biochim Biophys Acta. 2011;1808(6):1448–53.
99. Luik P, et al. The 3-dimensional structure of a hepatitis C virus p7 ion channel by electron microscopy. Proc Natl Acad Sci U S A. 2009;106(31):12712–6.
100. Gouaux E, Mackinnon R. Principles of selective ion transport in channels and pumps. Science. 2005;310(5753):1461–5.
101. Cuello LG, et al. Structural basis for the coupling between activation and inactivation gates in K(+) channels. Nature. 2010;466(7303):272–5.

102. Lunin VV, et al. Crystal structure of the CorA Mg2+ transporter. Nature. 2006;440(7085):833–7.
103. Hou X, Pedi L, Diver MM, Long SB. Crystal structure of the calcium release-activated calcium channel Orai. Science. 2012;338(6112):1308–13.
104. Sakai N, et al. Synthetic multifunctional pores: deletion and inversion of anion/cation selectivity using pM and pH. Org Biomol Chem. 2003;1(7):1226–31.
105. Gan SW, Surya W, Vararattanavech A, Torres J. Two different conformations in hepatitis C virus p7 protein account for proton transport and dye release. PLoS One. 2014;9(1):e78494.
106. Davies WL, et al. Antiviral activity of 1-adamantanamine (amantadine). Science. 1964;144(3620):862–3.
107. Hay AJ, Wolstenholme AJ, Skehel JJ, Smith MH. The molecular basis of the specific anti-influenza action of amantadine. EMBO J. 1985;4(11):3021–4.
108. Pinto LH, Holsinger LJ, Lamb RA. Influenza virus M2 protein has ion channel activity. Cell. 1992;69(3):517–28.
109. Wang C, Takeuchi K, Pinto LH, Lamb RA. Ion channel activity of influenza A virus M2 protein: characterization of the amantadine block. J Virol. 1993;67(9):5585–94.
110. Griffin S, et al. Genotype-dependent sensitivity of hepatitis C virus to inhibitors of the p7 ion channel. Hepatology. 2008;48(6):1779–90.
111. Jing X, et al. Functional studies indicate amantadine binds to the pore of the influenza A virus M2 proton-selective ion channel. Proc Natl Acad Sci U S A. 2008;105(31):10967–72.
112. Ohigashi Y, et al. An amantadine-sensitive chimeric BM2 ion channel of influenza B virus has implications for the mechanism of drug inhibition. Proc Natl Acad Sci U S A. 2009;106(44):18775–9.
113. Griffin SD, et al. A conserved basic loop in hepatitis C virus p7 protein is required for amantadine-sensitive ion channel activity in mammalian cells but is dispensable for localization to mitochondria. J Gen Virol. 2004;85(Pt 2):451–61.
114. Dev J, Bruschweiler S, Ouyang B, Chou JJ. Transverse relaxation dispersion of the p7 membrane channel from hepatitis C virus reveals conformational breathing. J Biomol NMR. 2015;61(3–4):369–78.
115. Daniels RS, et al. Fusion mutants of the influenza virus hemagglutinin glycoprotein. Cell. 1985;40(2):431–9.
116. Melikyan GB, Markosyan RM, Roth MG, Cohen FS. A point mutation in the transmembrane domain of the hemagglutinin of influenza virus stabilizes a hemifusion intermediate that can transit to fusion. Mol Biol Cell. 2000;11(11):3765–75.
117. Steinhauer DA, Wharton SA, Skehel JJ, Wiley DC. Studies of the membrane fusion activities of fusion peptide mutants of influenza virus hemagglutinin. J Virol. 1995;69(11):6643–51.
118. Helseth E, et al. Changes in the transmembrane region of the human immunodeficiency virus type 1 gp41 envelope glycoprotein affect membrane fusion. J Virol. 1990;64(12):6314–8.
119. Owens RJ, Burke C, Rose JK. Mutations in the membrane-spanning domain of the human immunodeficiency virus envelope glycoprotein that affect fusion activity. J Virol. 1994;68(1):570–4.
120. Shang L, Yue L, Hunter E. Role of the membrane-spanning domain of human immunodeficiency virus type 1 envelope glycoprotein in cell-cell fusion and virus infection. J Virol. 2008;82(11):5417–28.
121. Long Y, Meng F, Kondo N, Iwamoto A, Matsuda Z. Conserved arginine residue in the membrane-spanning domain of HIV-1 gp41 is required for efficient membrane fusion. Protein Cell. 2011;2(5):369–76.
122. Rotem E, Reuven EM, Klug YA, Shai Y. The transmembrane domain of HIV-1 gp41 inhibits T-cell activation by targeting multiple T-cell receptor complex components through its GxxxG motif. Biochemistry. 2016;55(7):1049–57.
123. Harrison SC. Viral membrane fusion. Nat Struct Mol Biol. 2008;15(7):690–8.
124. Weissenhorn W, Dessen A, Harrison SC, Skehel JJ, Wiley DC. Atomic structure of the ectodomain from HIV-1 gp41. Nature. 1997;387:426–30.

125. Pancera M, et al. Structure and immune recognition of trimeric pre-fusion HIV-1 Env. Nature. 2014;514(7523):455–61.
126. Chan DC, Kim PS. HIV entry and its inhibition. Cell. 1998;93(5):681–4.
127. Wei X, et al. Antibody neutralization and escape by HIV-1. Nature. 2003;422(6929):307–12.
128. Richman DD, Wrin T, Little SJ, Petropoulos CJ. Rapid evolution of the neutralizing antibody response to HIV type 1 infection. Proc Natl Acad Sci U S A. 2003;100(7):4144–9.
129. Chen J, et al. HIV-1 ENVELOPE. Effect of the cytoplasmic domain on antigenic characteristics of HIV-1 envelope glycoprotein. Science. 2015;349(6244):191–5.
130. Kovacs JM, et al. HIV-1 envelope trimer elicits more potent neutralizing antibody responses than monomeric gp120. Proc Natl Acad Sci U S A. 2012;109(30):12111–6.
131. Sanders RW, et al. A next-generation cleaved, soluble HIV-1 Env trimer, BG505 SOSIP.664 gp140, expresses multiple epitopes for broadly neutralizing but not non-neutralizing antibodies. PLoS Pathog. 2013;9(9):e1003618.
132. Chen B, et al. Structure of an unliganded simian immunodeficiency virus gp120 core. Nature. 2005;433(7028):834–41.
133. Kwong PD, et al. Structures of HIV-1 gp120 envelope glycoproteins from laboratory-adapted and primary isolates. Struct Fold Des. 2000;8(12):1329–39.
134. Kwong PD, et al. Structure of an HIV gp120 envelope glycoprotein in complex with the CD4 receptor and a neutralizing human antibody. Nature. 1998;393:648–59.
135. Huang CC, et al. Structure of a V3-containing HIV-1 gp120 core. Science. 2005;310(5750):1025–8.
136. Tan K, Liu J-H, Wang J-H, Shen S, Lu M. Atomic structure of a thermostable subdomain of HIV-1 gp41. Proc Natl Acad Sci U S A. 1997;94:12303–8.
137. Caffrey M, et al. Three-dimensional solution structure of the 44kDa ectodomain of SIV gp41. EMBO J. 1998;17:4572–84.
138. Julien JP, et al. Crystal structure of a soluble cleaved HIV-1 envelope trimer. Science. 2013;342(6165):1477–83.
139. Lyumkis D, et al. Cryo-EM structure of a fully glycosylated soluble cleaved HIV-1 envelope trimer. Science. 2013;342(6165):1484–90.
140. MacKenzie KR, Prestegard JH, Engelman DM. A transmembrane helix dimer: structure and implications. Science. 1997;276(5309):131–3.
141. Bocharov EV, et al. Spatial structure of the dimeric transmembrane domain of the growth factor receptor ErbB2 presumably corresponding to the receptor active state. J Biol Chem. 2008;283(11):6950–6.
142. Langosch D, Arkin IT. Interaction and conformational dynamics of membrane-spanning protein helices. Protein Sci. 2009;18(7):1343–58.
143. Falson P, et al. Hepatitis C virus envelope glycoprotein E1 forms trimers at the surface of the Virion. J Virol. 2015;89(20):10333–46.
144. Cleverley DZ, Lenard J. The transmembrane domain in viral fusion: essential role for a conserved glycine residue in vesicular stomatitis virus G protein. Proc Natl Acad Sci U S A. 1998;95(7):3425–30.
145. West JT, Johnston PB, Dubay SR, Hunter E. Mutations within the putative membrane-spanning domain of the simian immunodeficiency virus transmembrane glycoprotein define the minimal requirements for fusion, incorporation, and infectivity. J Virol. 2001;75(20):9601–12.
146. Knowles DP Jr, et al. Structure and genetic variability of envelope glycoproteins of two antigenic variants of caprine arthritis-encephalitis lentivirus. J Virol. 1991;65(11):5744–50.
147. Rice NR, et al. Synthesis and processing of the transmembrane envelope protein of equine infectious anemia virus. J Virol. 1990;64(8):3770–8.
148. Sonigo P, et al. Nucleotide sequence of the visna lentivirus: relationship to the AIDS virus. Cell. 1985;42(1):369–82.
149. Pietschmann T, Zentgraf H, Rethwilm A, Lindemann D. An evolutionarily conserved positively charged amino acid in the putative membrane-spanning domain of the foamy virus envelope protein controls fusion activity. J Virol. 2000;74(10):4474–82.

150. Ciczora Y, et al. Contribution of the charged residues of hepatitis C virus glycoprotein E2 transmembrane domain to the functions of the E1E2 heterodimer. J Gen Virol. 2005;86(Pt 10):2793–8.
151. Sun ZY, et al. HIV-1 broadly neutralizing antibody extracts its epitope from a kinked gp41 ectodomain region on the viral membrane. Immunity. 2008;28(1):52–63.
152. Kim M, et al. Antibody mechanics on a membrane-bound HIV segment essential for GP41-targeted viral neutralization. Nat Struct Mol Biol. 2011;18(11):1235–43.
153. Sakaguchi T, Tu Q, Pinto LH, Lamb RA. The active oligomeric state of the minimalistic influenza virus M2 ion channel is a tetramer. Proc Natl Acad Sci U S A. 1997;94(10):5000–5.
154. Balannik V, Lamb RA, Pinto LH. The oligomeric state of the active BM2 ion channel protein of influenza B virus. J Biol Chem. 2008;283(8):4895–904.
155. Clarke D, et al. Evidence for the formation of a heptameric ion channel complex by the hepatitis C virus p7 protein in vitro. J Biol Chem. 2006;281(48):37057–68.
156. Lu JX, Sharpe S, Ghirlando R, Yau WM, Tycko R. Oligomerization state and supramolecular structure of the HIV-1 Vpu protein transmembrane segment in phospholipid bilayers. Protein Sci. 2010;19(10):1877–96.
157. Gonzalez ME, Carrasco L. The human immunodeficiency virus type 1 Vpu protein enhances membrane permeability. Biochemistry. 1998;37(39):13710–9.
158. Lu W, et al. Severe acute respiratory syndrome-associated coronavirus 3a protein forms an ion channel and modulates virus release. Proc Natl Acad Sci U S A. 2006;103(33):12540–5.
159. Verdia-Baguena C, et al. Analysis of SARS-CoV E protein ion channel activity by tuning the protein and lipid charge. Biochim Biophys Acta. 2013;1828(9):2026–31.
160. Moyer CL, Nemerow GR. Viral weapons of membrane destruction: variable modes of membrane penetration by non-enveloped viruses. Curr Opin Virol. 2011;1(1):44–9.
161. Agirre A, Barco A, Carrasco L, Nieva JL. Viroporin-mediated membrane permeabilization. Pore formation by nonstructural poliovirus 2B protein. J Biol Chem. 2002;277(43):40434–41.
162. Sudarshan SR, Schlegel R, Liu X. The HPV-16 E5 protein represses expression of stress pathway genes XBP-1 and COX-2 in genital keratinocytes. Biochem Biophys Res Commun. 2010;399(4):617–22.
163. Suprynowicz FA, et al. HPV-16 E5 oncoprotein upregulates lipid raft components caveolin-1 and ganglioside GM1 at the plasma membrane of cervical cells. Oncogene. 2008;27(8):1071–8.
164. Kabsch K, Alonso A. The human papillomavirus type 16 (HPV-16) E5 protein sensitizes human keratinocytes to apoptosis induced by osmotic stress. Oncogene. 2002;21(6):947–53.
165. Romani G, et al. Viral encoded potassium ion channel is a structural protein in the chlorovirus Paramecium bursaria chlorella virus-1 (PBCV-1) Virion. J Gen Virol. 2013;94(Pt 11):2549.